Ph.D. Dissertation of Pharmacy

Structural and functional studies on human ChaC in glutathione metabolism

인간 유래 ChaC 단백질의 glutathione 대사에서 구조및 기능이 대한 연구

February 2020

Graduate School of Pharmacy
Seoul National University
Pharmaceutical bioscience Major

Nguyen Thi Kim Yen

Abstract

Glutathione (GSH) degradation plays an essential role not only in the GSH homeostasis but also in housekeeping functions, which regulate cell survival especially in cancer cells. Among human GSH degradation enzymes, cytosolic ChaC1 and ChaC2 enzymes act on GSH to form 5-L-oxoproline and Cys-Gly specifically in cytosol and share 60% sequence similarities. Here, I report the crystal structures of ChaC2 in two different conformations and compare structural features with other known ɣ-glutamylcyclotransferase enzymes. The unique domain-swapped loop of ChaC2 seems to function as a gate to achieve specificity for GSH binding and regulate the constant GSH degradation rate. Intensive structural and biochemical analyses of ChaC2 revealed that Glu74 and Glu83 play crucial roles in directing the assembly of the swapping dimer and in modulating the enzyme activity. Based on the docking study of GSH to ChaC2 and binding assay, I propose a substrate binding mode and catalytic mechanism. I also found that overexpression of ChaC2, but not ChaC2 E74Q or ChaC2 E83Q, significantly promoted breast cancer cell line proliferation, suggesting that the GSH degradation role of ChaC protein plays a role in breast cancer cell growth. My structural and functional analyses of ChaC2 will contribute to the development of modulators in the ChaC family, which could effectively regulate the progression of GSH degradation-related diseases and cancers.

Keyword: ɣ-glutamylcyclotransferase; GSH degradation; swapping domain; breast cancer; crystal structure; MAD Phasing

Student Number: 2013-23934

Table of Contents

List of Tables

List of Figures

Abbreviations

ASU	asymmetric unit
DTT	1,4-dithiothreitol
GGACT	ɣ-glutamylaminecyclotransferase
GGCT	ɣ-glutamylcyclotransferase
GSH	glutathione
LB	Luria-Bertani
MAD	Multiple wavelength anomalous dispersion
MR	molecular replacement
PMSF	phenylmethylsulfonyl fluoride
PEG	polyethylene glycol
PDB	Protein Data Bank
SeMet	selenomethionine
SA	solvent accessibility
IPTG	1-thio-ß-D-galactopyranoside
TCEP	Tris (2-carboxyethyl) phosphine

I. Introduction

1. Study Background

GSH is a crucial tripeptide (ɣ-glutamyl-cysteinyl glycine) that participates in diverse cellular functions, including cellular detoxification and redox signaling [1], cell proliferation, and apoptosis [2] (Figure 1). Disturbances of GSH homeostasis have been observed in many pathophysiological contexts [3]. In particular, aberrant GSH levels are correlated with tumor initiation, progression, and chemotherapeutic resistance [4, 5]. As such, it has drawn attention in relation to cancer metabolism biology and treatment [4].

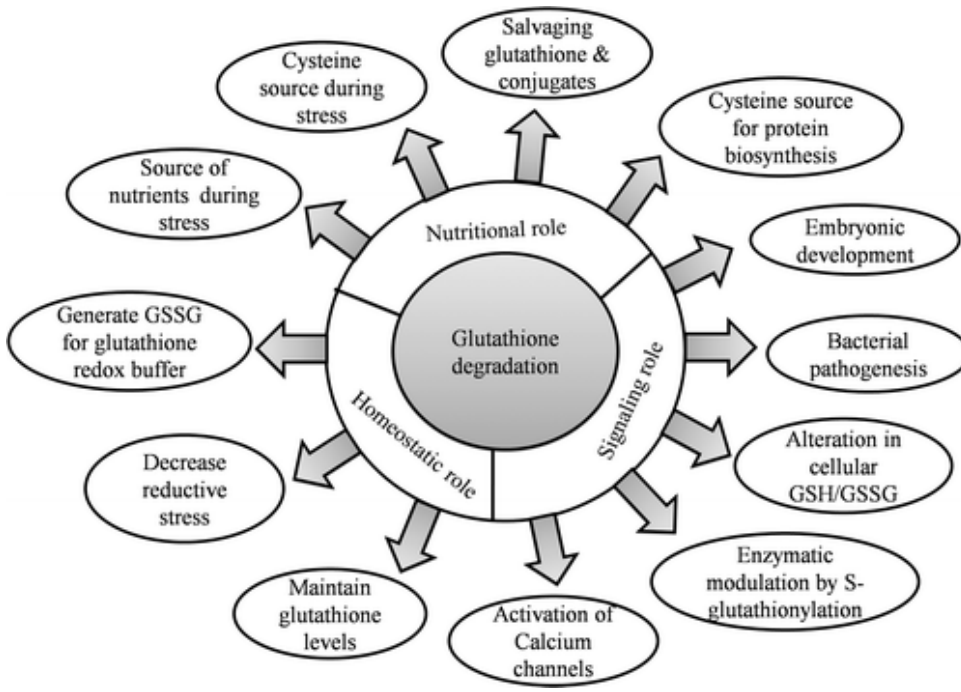

Figure 1. The cellular roles of glutathione degradation

The GSH homeostasis is balanced by the GSH biosynthesis, transport and efflux of GSH, GSH-acting enzymes, and GSH degradation (Figure2). GSH is mainly synthesized by two enzymes ATP-dependent ligase and glutamate cysteine ligase [6]. Although the contribution of GSH biosynthesis has been well studied, the GSH degradation pathway, which involves the initial cleavage of GSH, remains poorly understood. Several enzymes responsible for the GSH degradation have been increasingly studied [6]. The human γ-glutamyltranspeptidase enzyme family comprises the first reported enzymes responsible for the GSH degradation pathway in the extracellular or vacuolar environment [7], which are able to cleave various γ-glutamyl substrates, including GSH-S-conjugate, GSSG (oxidized GSH), and γ-glutamyl compounds [8, 9]. Recently, two isoform enzymes, ChaC1 and ChaC2, belonging to the γ-glutamylcyclotransferase (GGCT) family have drawn attention due to their ability to cleave the γ-glutamyl group of glutathione, resulting in 5-L-oxoproline and glutamyl-cysteinyl (Cys-Gly) specifically in the cytosol [10-14].

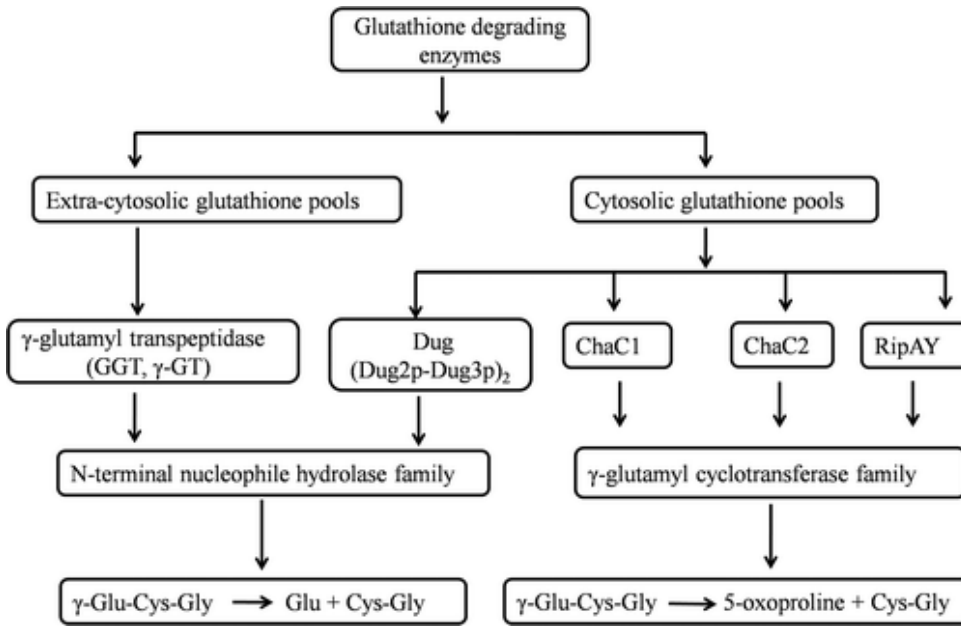

Figure 2. Enzymes of glutathione degradation

The different enzymes of glutathione degradation classified on the basic of the glutathione pools they act on and on their enzymatic activities.

In humans, the GGCT-fold enzyme family is composed of γ-glutamylcyclotransferase (GGCT), γ-glutamylaminecyclotransferase (GGACT), and glutathione-specific γ-glutamylcyclotransferase (ChaC1 and ChaC2). Despite their low sequence identities, GGCT-fold enzymes exhibit a similar structural fold for their catalysis, including an YGSL motif and common catalytic Glu residues, as well as unique features, especially in the vicinity of the active site, which specifies the substrate repertoire [11, 14]. The GGCT targets on γ-glutamyl derivatives, such as GSH [11] and GGACT, catalyzes γ-glutamylamines [12]. Interestingly, ChaC enzymes specifically act on GSH [15].

Three-dimensional domain swapping is a phenomenon wherein one domain of a monomer is exchanged with an identical domain from a second monomer. Domain swapping has been reported to play several roles in the structural organization of proteins [16], preventing proteins from forming cytotoxic aggregates [17], as well as regulating protein function [18]. Several factors, including conformational straining of closed monomers [19] and structural flexibility in the hinge loop region [20], affect domain-swapping progress. However, the physiological mechanism of this progress is still poorly understood [21, 22].

To date, two cytosolic ChaC isoforms, ChaC1 and ChaC2, have been identified in most mammalian tissues [13]. ChaC1 and ChaC2 share a 60% sequence identity but their physiological expression and catalytic efficiency are quite different [13]. ChaC2 exhibits a 10-to 20-fold lower catalytic efficiency than ChaC1 [13] and is constitutively expressed and involved in the "housekeeping" GSH metabolism [10]. In contrast, ChaC1 is an inducible enzyme that is expressed transiently in response to specific stress conditions or in tumor cells [13, 23, 24]. Recently, it was reported that ChaC2 directly targets GSH and regulates ChaC1 in order to control the GSH metabolism sustainably [10]. ChaC2 is known to affect the expression of the antioxidant master regulator nuclear erythroid-2-like factor (Nrf2) and glutamate cysteine ligase in the ChaC1-independent pathways [10].

ChaC1 is known as a novel prognostic marker in many types of cancer [23,

25, 26]. The overexpression of ChaC1 has been found to result in the depletion of GSH, as well as enhanced apoptosis in human embryonic kidney cells (HEK293) [26, 27]. Interestingly, ChaC1-overexpressing Hs578T breast cancer and HOC-7 ovarian carcinoma cell lines exhibited increased migration and proliferation [25]. Recent studies on ChaC2 have also shown differential functions in various situations. For example, ChaC2 is downregulated in gastric and colorectal cancer, and the overexpression of ChaC2 has been shown to inhibit cell proliferation [28]. On the contrary, the downregulation of ChaC2 resulted in the decrease of cell proliferation and the induction of cell death in human embryonic stem cells, and ChaC2 knockdown decreased the teratoma size and enriched teratoma adipocytes [10]. In addition, ChaC2 is exclusively up-regulated in ovarian cancer cells (OV-90, OVCAR3, SKOV3, TOV-21, TOV-112, and TOV-155) treated with drugs including cisplatin, paclitaxel, and topotecan [29]. GSH degradation is a well-known factor in apoptosis, cancer execution, and chemotherapeutic resistance in many cancer cells [23, 30], however, the correlation between ChaC family functions, GSH depletion, and breast cancer cell proliferation remains poorly understood [25].

2. Purpose of Research

To gain insights into how the ChaC enzymes specifically work on GSH and mediate their functions, homology models of ChaC1 based on the GGCT structure [14, 15] and the crystal structure of yeast ChaC2 have been elucidated [13]. However, the structural features for the substrate specificities of the ChaC enzymes have not yet been fully described.

In this research, I wanted to determine the crystal structure of ChaC2 and ChaC1 by X-ray Crystallography. I solved the structure of ChaC2 and found that ChaC2 existed both domain-swapping homodimer and closed monomer conformation. To further investigate the structure-function relationships, I conducted enzymatic assays, cell proliferation tests, multiple structural alignments, and molecular docking simulations. I identified the catalytic

residues of ChaC2 responsible for the GSH degradation activity and proposed that a domain-swapping phenomenon may regulate the GSH degradation function. I associated the GSH degradation pathway mediated by ChaC2 in the regulation of the antioxidant defense in MCF-7 breast cancer cell lines and suggested a GSH degradation reaction mechanism. Taken together, my structural and biochemical analysis provide an insight into the cytosolic GSH degradation pathway. My findings would shed a light for the design of novel modulators of ChaC family proteins in breast cancer, which often cause issues resulting in drug resistance.

II. Materials and methods

1. Bioinformatics analysis

The amino acid sequences of ChaC1, ChaC2, GGCT, and GGACT were obtained from UniProt [31]. Sequence alignments were performed using Clustal Omega [32] and visualized with ESPRIPT3 [33]. The residues for substituted methionine were selected based on the secondary structure combined with solvent accessibility (SA) prediction, and the conserved sequence information of ChaC2 from various organisms [34]. The secondary structure and SA were predicted using the *PSIPRED* [35] and the *SABLE* server [36], respectively.

ChaC2 gene expression in different tissues was analyzed and visualized using the Oncomine database [37] (https://www.oncomine.org). The mRNA expression of ChaC2 in clinical invasive ductal breast carcinoma specimens were compared with that in normal tissue using Student's t- test to generate the p-value. The cut-off p-value and fold change were defined as 0.05 and 1.3, respectively. Turashvili Breast, Karnoub Breast, and TCGA Breast were the main sources of the data that was analyzed. The Kaplan–Meier method was used to analyze the survival rate as a function of time. The Kaplan–Meier plot was acquired from the online Kaplan–Meier plotter (Breast Cancer) [31] (https://kmplot.com). The survival differences were conducted using the log-rank test.

2. Cloning and protein production

2.1. Cloning and protein production of ChaC2

The cDNAs for human ChaC2 was obtained from the Korean Human Gene Bank. The ChaC2 genes was amplified by polymerase chain reaction (PCR) and inserted into pET-15b vector between the BamHI and XhoI restriction enzyme sites with a hexa-histidine tag at the N-terminus. The vector was transformed into the Escherichia coli C41 (DE3) strain. The transformed cells were incubated at 37 ℃ in Luria-Bertani (LB) medium containing

ampicillin until the OD600 reached 0.6. Then, 0.4 mM IPTG (1-thio-ß-D-galactopyranoside) was added. The cells were incubated for further 20 h at 18 ℃ and harvested by centrifugation at 6,000 × g for 10 min. The harvested cells were lysed by sonication for 10 min at 60% amplitude (SONICS, CT, USA) in buffer containing 20 mM Tris-HCl (pH 7.5), 500 mM NaCl, 35 mM imidazole and 1 mM phenylmethylsulfonyl fluoride (PMSF). The lysates were centrifuged at 30,000 x g for 1h at 4 ℃. The resulting supernatants were filtered using a 0.45 μM syringe filter device (Sartorius, Göttingen, Germany) and loaded onto a 5-ml HiTrap Chelating HP column (GE Healthcare, Chicago, IL, USA) pre-charged with Ni2+ and equilibrated with buffer containing 20 mM Tris-HCl (pH 7.5), 500 mM NaCl, and 35 mM imidazole. After washing with the buffer used in equilibration, the retained proteins were eluted by the addition of an increasing gradient of buffer containing 20 mM Tris-HCl (pH 7.5), 500 mM NaCl, and 1 M imidazole. The eluted fractions were dialyzed with buffer containing 20 mM Tris-HCl (pH 7.2) and 30 mM NaCl before loading onto a 5 ml HiTrap Q HP column (GE Healthcare). The bound proteins were eluted by adding an increasing gradient of buffer containing 20 mM Tris-HCl (pH 7.2) and 1 M NaCl. The eluted fractions were pooled and loaded onto a HiLoad 16/600 Superdex 75 pg column (GE Healthcare) equilibrated with buffer containing 20 mM Tris-HCl (pH 7.1), 150 mM NaCl, 5 mM 1, 4-dithiothreitol (DTT), and 2% glycerol. The purities of the protein fractions were confirmed by SDS-PAGE (Figure 3)

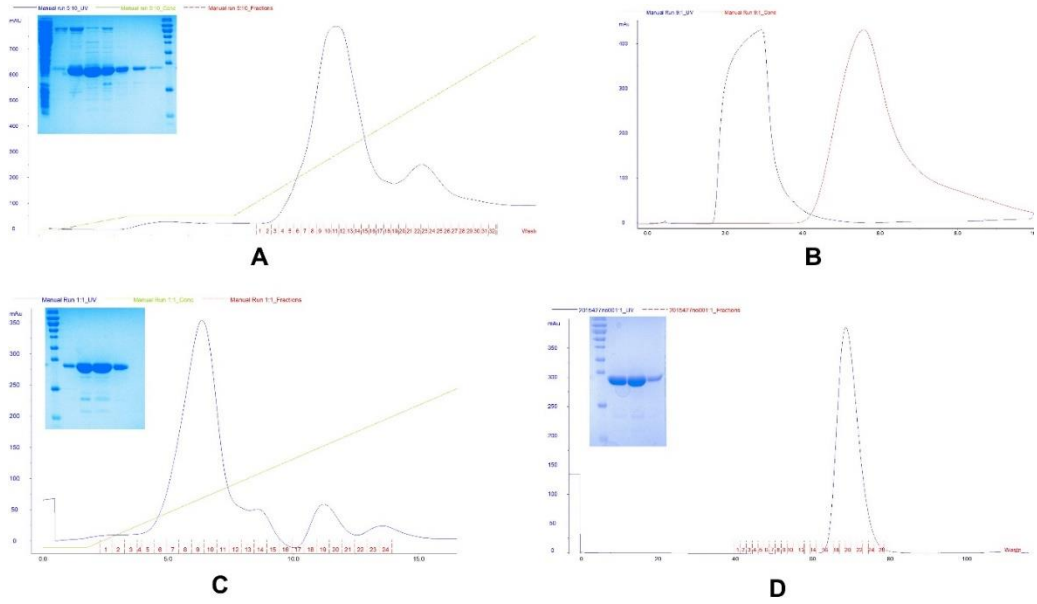

Figure 3. Purification of ChaC2 protein.

Ni2+ affinity chromatography (A), desalting chromatography (B), anion exchange chromatography (C), and size-exclusion chromatography (D). Purity of the protein factions was checked by SDS-PAGE after each purification step.

The oligomeric state of the proteins was characterized by size-exclusion chromatography with HiLoad 16/600 Superdex 75 pg column (GE Healthcare) in the same buffer, at a constant flow of 1 mL/min. The column was calibrated under identical running conditions with molecular weight standard mixture (thyroglobulin 670 kDa, ɣ-globulin 158 kDa, ovalbumin 44 kDa, myoglobin 17 kDa, and vitamin B_{12} 1.35 kDa).

For selenomethionine (SeMet) incorporation, a ChaC2 L21M, L118M, and L181M mutant was overexpressed in *Escherichia coli* B834 (DE3) cells. The ChaC2-mutant transformed cells were grown in M9 minimal medium supplemented with L-selenomethionine and other amino acids. Protein preparation steps were the same with native proteins. A protease cocktail (Calbiochem, San Diego, CA, USA) and 10 mM 2-mercaptoethanol were supplemented in the buffer used in cell lysis. Finally, 5 mM DTT was added to all the purification buffers.

2.2. Cloning and protein production of ChaC1

The cDNAs for human ChaC1 was obtained from the Korean Human Gene Bank. The construct of ChaC1 (42-222) was cloned into pET-21a vector between the BamHI and NdeI restriction enzyme sites with a hexa-histidine tag at the C-terminus. The Chac1 protein was overexpressed in the *Escherichia coli* BLR (DE3) strain. The transformed cell was grow at 37 ℃ to an OD_{600} of 0.5 in LB media containing ampicillin. Protein expression was induced by 0.5 mM IPTG for 16 h before harvesting. The harvested cells were suspended in buffer containing 20 mM Tris-HCl (pH 7.5), 500 mM NaCl, 35 mM imidazole, and 1 mM PMSF and then lysed by sonication. The lysates were centrifuged at 30,000 x *g* for 1 h at 4 ℃. The supernatants were filtered and loaded onto a 5-ml HiTrap Chelating HP column pre-charged with Ni^{2+} and equilibrated with buffer containing 20 mM Tris-HCl (pH 7.5), 500 mM NaCl, and 35 mM imidazole. After washing with the buffer used in equilibration, the retained proteins were eluted by an increasing gradient of buffer containing 20 mM Tris-HCl (pH 7.5), 500 mM NaCl, and 1 M imidazole. The eluted fractions were dialyzed with buffer containing 20

mM Tris-HCl (pH 8.0), 30 mM NaCl, and 10 mM TCEP before loading onto a 5 ml HiTrap Q HP column. The proteins were eluted by a gradient of buffer containing 20 mM Tris-HCl (pH 8.0), 1 M NaCl, and 10 mM TCEP. The eluted fractions were pooled and loaded onto a HiLoad 16/600 Superdex 75 pg column equilibrated with buffer containing 20 mM MES (pH 6.5), 200 mM NaCl, and 5 mM DTT. The purities of the protein fractions were confirmed by SDS-PAGE (Figure 4)

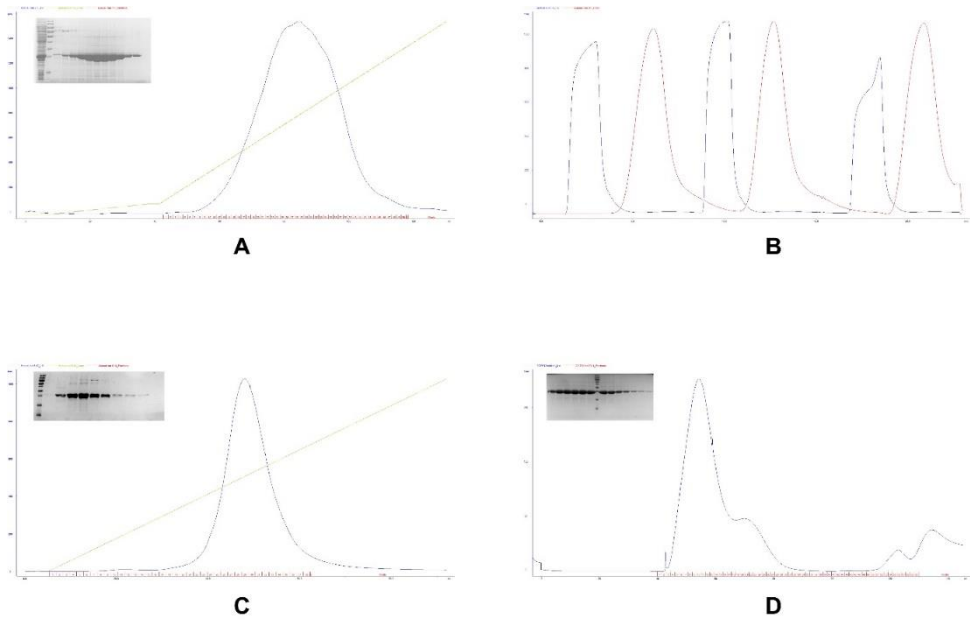

Figure 4. Purification of ChaC1.

Ni2+ affinity chromatography (A), desalting chromatography (B), anion exchange chromatography (C), and size-exclusion chromatography (D). Purity of the protein factions was checked by SDS-PAGE after each purification step.

3. Mutagenesis

ChaC2 mutants were generated using the QuickChange II Site-Directed Mutagenesis Kit (Agilent Technologies). The recombinant pET-15b vector with ChaC2 gene was used as a template for mutagenesis. The mutant vectors were sequenced to confirm the presence of the desired mutation.

4. Crystallization

4.1. Crystallization of ChaC2

The crystallization conditions for ChaC2 were screened using commercial screening kits (Hampton Research). The ChaC2 crystals were grown by using the vapor diffusion hanging drop method with a reservoir solution containing 14% (w/v) polyethylene-glycol 8,000 (PEG 8000), 14% ethylene glycol, and 100 mM HEPES (pH 7.5) at 22 ℃. The crystals of ChaC2 L21M, L118M, and L181M mutant and its SeMet-derivative were grown using a modified crystallization condition containing 14% (w/v) PEG 8,000 and 100 mM Tris (pH 8.0) supplemented with 5% (w/v) PEG 200 for the ChaC2 mutant, and 2% pentaerythritol ethoxylate (3/4 EO/OH) for Semet-derivative, respectively. The crystals of ChaC2 E83Q and E74Q were grown with 3 M sodium acetate trihydrate (pH 7.0). The crystals were improved with the addition of 10 mM GSH or 5-L-oxoproline to the crystallization solution (Figure 5)

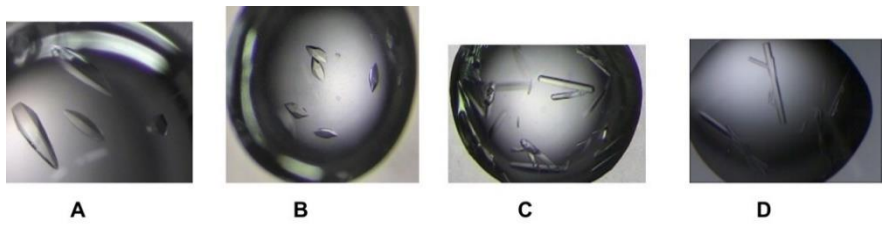

Figure 5. Crystals of human ChaC2.

ChaC2 (**A**), ChaC2 Semet (**B**), ChaC2 E74Q (**C**), and ChaC2 E83Q (**D**) crystals are observed under microscopy.

4.2. Crystallization of ChaC1

The crystallization conditions for ChaC1 were screened using commercial screening kits. The ChaC1 crystals were grown by using the sitting-drop vapor-diffusion method with a reservoir solution containing 10% (*v/v*) 2-methyl-2, 4-pentadiol and 100 mM BICINE sodium (pH 9.0) at 22 ℃ (Figure 6A). The crystals were checked under UV spectroscopy to confirm protein crystals before further optimization (Figure 6B). However, the crystals were damaged and destroyed after 1 week. Unfortunately, I was not able to reproduce the crystal for further structure determination experiment later on (Figure 6C).

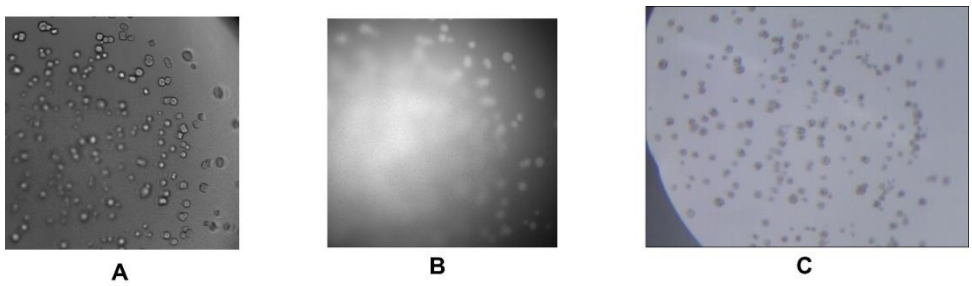

Figure 6. Crystals of human ChaC1.

ChaC1 crystals are observed under microscopy (A), ChaC1 crystals are observed under UV microscopy (B), and ChaC1 crystals are observed under microscopy after 1 week (C).

5. X-ray diffraction data collection, structure determination, and refinement

Before the collection of the X-ray diffraction data, the ChaC2 crystals were cryoprotected in reservoir solution supplemented with 26% ethylene glycol (for the ChaC2 of ChaC2 L21M, L118M, and L181M mutant and SeMet-labeled crystals) or 20% glycerol (for ChaC2 E83Q and ChaC2 E74Q crystals) before flash freezing in a nitrogen-gas stream at 100 K. The X-ray diffraction data were collected on the beamlines 5C and 7A at the Pohang Accelerator Laboratory (Pohang, Korea) or Spring-8 (Osaka, Japan). The collected data were indexed, merged, and scaled using the HKL2000 package [38]. SeMet-labeled crystals were scanned the anomalous signal to determine the anomalous peak, edge, and remote wavelengths before collecting the data (Figure 7)

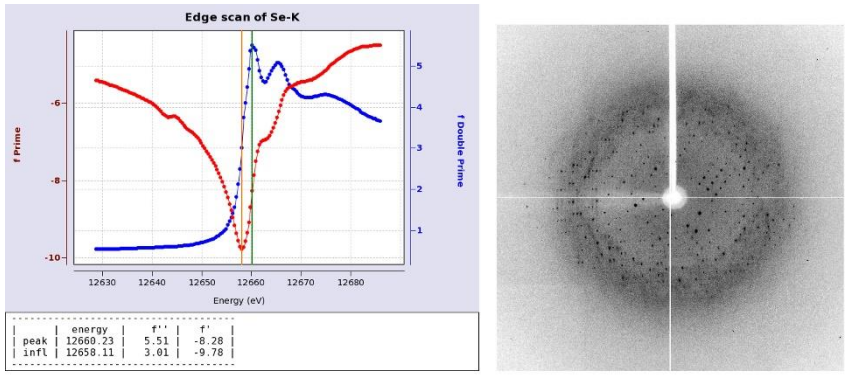

Figure 7. Anomalous signal scanning (A) and X-ray diffraction pattern (B) of ChaC2 SeMet-labeled crystals

The initial model of Seleno-derived crystal of ChaC2 L21M, L118M, and L181M mutant was obtained by multiple-wavelength anomalous dispersion (MAD) method using the *Autosol* program in *Phenix* software package [39]. The protein structure model was constructed using the *Autobuild* routine in the *Phenix* software package. The initial model from the MAD method was used as a template for molecular replacement using the *Phaser* program [40]. The ChaC2 model without a loop2 region was used as a temple for the ChaC2 E74Q structure determination by molecular replacement (MR) method. The ChaC2 E74Q model was used as template for the ChaC2 E83Q structure determination. Further iterative manual building and the refinement of models were carried out using *Coot* [41] and *CCP4i* [42]. The quality of the overall geometry and conformation were validated using the *MolProbity* program [43]. Before PDB (Protein Data Bank) deposition, *PDB-redo* [44] was performed to complete the structures.

6. Preparation of ChaC2-overexpressing cells

HEK293, MCF-7, and MDA-MB-231 breast cancer cell lines were donated by Professor Lee Sang Kook's laboratory. The cells were cultured in Dulbecco's Modified Eagle's Medium (HyClone, Hudson, NH, USA) supplemented with 10% fetal bovine serum and 1% penicillin/streptomycin (Gibco, Waltham, MA, USA) in a humidified atmosphere of 5% CO_2 at 37 °C. The ChaC2, ChaC2 E74Q, and ChaC2 E83Q were cloned into pEGFP-C3 vectors using the KpnI and BamHI restriction enzymes. The recombinant plasmids were transfected into the cells using polyethylenimine reagent (Sigma Aldrich, Saint Louis, MO, USA) according to the manufacturers' protocol at a rate of 2:1 (μL of polyethylenimine/ g of plasmid DNA). The transfection efficiency was examined using a fluorescent microscope (Niko, Tokyo, Japan). To verify the successful overexpression of ChaC2 in these cell lines, western blotting was performed with the transfected cells lysates. The exogenous protein expression levels of GFP-ChaC2 were compared to those of an empty pEGFP-C3 vector (Mock).

7. GSH degradation activity of ChaC enzymes by LC-MS

For LC-MS/MS measurement, different concentration of substrate (20, 200 μM) GSH were added to 1 μM protein of ChaC2 and ChaC1 in the buffer containing phosphate-buffered saline and 1 mM DTT) for final 100 μL. Analytical samples were prepared by centrifuging the heat-inactivated reaction mixtures at 20,000 x *g* for 10 min and diluting the supernatants 50 times (*v*/*v*) with water. 5-L-oxoproline after reactions were quantified using a liquid chromatography-tandem mass spectrometry (LC-MS/MS) system equipped with a binary pump, a thermostatic column compartment, a thermostat, and an autosampler (1260 Infinity-6430 Triple Quad; Agilent Technologies, Palo Alto, CA, USA). Chromatographic separation was performed using a Kinetex C18 column (2.6 μ, 100 Å, 100 x 4.6 mm; Phenomenex, CA, USA) with a C18 guard column (4 x 2.0 mm; Phenomenex). The isocratic mobile phase consisted of acetonitrile and water with 0.2% (v/v) formic acid (30:70, *v*/*v*), and the elution was conducted at a flow rate of 0.4 mL/min. The injection volume was 5.0 μL, and the total run time was 3.0 min. Mass spectrometric detection was achieved using the multiple reaction monitoring (MRM) mode with positive electrospray ionization (ESI). The ESI source settings were manually optimized; gas temperature, gas flow, nebulizer pressure, and capillary voltage were 350 °C, 11 L/min, 30 psi (nitrogen), and 3,000 V, respectively. The fragmentation transitions were *m*/*z* 130.0 to 84.0 for 5-L-oxoproline. The fragmentor voltage and collision energy were 90 V and 10 eV for 5-L-oxoproline. The dwell time and the mass filter for each analyte was set at 50 ms and unit resolution, respectively. The data acquisition and processing were performed by using MassHunter Workstation Software Quantitative Analysis (Version B.05.00; Agilent Technologies).

We quantified the concentration 5-L-oxoproline based on the standard curves. Enzymatic activities were determined by the release amount of 5-L-oxoproline after reaction. For all assays, the reaction mixture without enzyme was used as background. The reactions were done triple.

8. GSH assays

The Mock, ChaC2, ChaC2 E74Q, and ChaC2 E83Q overexpressed HEK293 cells were harvested and lysed as described in a previous study [45]. Briefly, 1×10^6 cells were suspended in 25 µL of assay buffer with 175 µL of 5% meta-phosphoric acid before sonicating for 2 min with vortexing every 30 s. The sonicated cells were centrifuged at 12,000 × *g* for 10 min at 4 ℃ before the assay. The supernatant samples were then diluted 50-fold and the concentration of GSH was immediately measured using the OxiSelect Total Glutathione Assay Kit (Cell Biolabs, San Diego, CA, USA). First, 50 µL of the buffer, standards, and samples were transferred to 96-well plates. Then, 50 µL of 5, 5'-dithiobis (2-nitrobenzoic acid) solution, 50 µL of reductase, and 50 µL of nicotinamide adenine dinucleotide phosphate were serially added. Immediately after, the absorbance of the samples at 412 nm was measured every 30 s for 2 min using a microplate reader (Spectra MAX M5; Molecular Devices, Sunnyvale, Calif, USA). The GSH concentration was calculated from the absorbance. All measurements were conducted in triplicate.

For the in vitro enzymatic assay, 0.1 g/L of purified ChaC1, ChaC2, ChaC2 E74Q, and ChaC2 E83Q were incubated with 5 mM GSH in 100 µL at 37 ℃ for 1 h. Then, the reactants were heat-inactivated at 95 ℃ for 5 min. The samples were 80 times diluted before measuring the GSH concentration.

9. Viability assays (MTT assays)

The Mock, ChaC2, ChaC2 E74Q, and ChaC2 E83Q overexpressed breast cancer cells were seeded onto 96-well plates at a density of 1×10^4 cells/well. After 48 h, 10 µL of the EZ-CYTOX solution from the Cell Viability, Proliferation & Cytotoxicity Assay Kit (DoGen, Seoul, Korea) was added to 100 µLof cell culture per well and incubated for 4 h for color development. The absorbance was measured at 450 nm to determine the number of viable cells. Each assay was performed at least three times.

10. Colony-forming assays

The transfected cells were seeded at a density of 1,000 cells/well on 6-well plates and allowed to grow for 2 weeks. The colonies were fixed with 100% methanol, stained with 0.005% crystal violet, and counted. The experiments were repeated three times.

11. Immunoblotting

The cellular proteins were extracted using cell lysis buffer containing 20 mM Tris-HCl (pH 7.5), 150 mM NaCl, 0.1 mM ethylenediaminetetraacetic acid, 0.1% Triton X-100, and protease inhibitor cocktail (Calbiochem). The total protein (20 μg) was separated via SDS-PAGE and electroblotted onto a PVDF membrane. The membrane was incubated overnight with the corresponding primary antibodies, followed by the secondary antibody conjugated to horseradish peroxidase at 4 ℃. Visualization was performed using ECL plus (GE Healthcare) and LAS-4000 (GE Healthcare). Anti-GFP (B-2, sc-9996) and anti-β-actin (I-19, sc-1616) antibodies were purchased from Santa Cruz Biotechnology, Oregon, USA.

12. Docking study

The crystal structure of ChaC2 E74Q and GGACT were used to calculate the binding energies of the GSH and 5-L-oxoproline to the protein. The calculation was implemented using *AutoDock Vina* software [46] with a grid map defined in $40 \times 40 \times 40$ Å^3 dimensions to contain the proposed active sites. The conformations of the ligands and receptors were fixed. The program was run in score mode with an exhaustiveness value of 20.

13. Surface plasmon resonance experiment

Surface plasmon resonance (SPR) binding assays were performed using a carboxymethyl dextran (CM5) sensor chip on a Biacore T200 instrument (GE Healthcare). The amine coupling for ligand immobilization was performed at a flow rate of 5 μL/min. The chip was activated with a mixture

of *N*-hydroxysuccinimide and *N*-Ethyl-N'-(dimethylaminopropyl) carbodiimide hydrochloride at a ratio of 1:1 for 400 s. Then, 13.3 μg/mL of ChaC2, ChaC2 E74Q, ChaC2 E83Q, and ChaC2 E74Q E83Q were diluted in 10 mM sodium acetate (pH 5.5) and injected until the immobilization level reached at 3,000 RU. The remaining activated carboxyl groups were deactivated with 1 M ethanolamine at pH 8.5 for 400 s. The control experiment in reference flow cells was treated identically with BSA (bovine serum albumin) protein. The multi-cycle analysis was performed at a flow rate of 30 μL/min. GSH at concentrations of 1.95, 3.91, 7.81, 15.63, 31.25, and 62.50 μM in running buffer (150 mM NaCl, 10 mM HEPES-NaOH pH 7.2, 0.005% p20) was injected over the chip for 240 s, followed by dissociation for 600 s in a separate analysis cycle. The sensor chip surface was regenerated with 5 mM NaOH between cycles. Data were fitted using the simple bimolecular 1:1 Langmuir isotherm binding model. The equilibrium dissociation constant (K_D) was determined using Biacore T200 evaluation software 3.0 (GE Healthcare).

14. Statistical analysis

All statistical results are presented the mean ± standard error of the mean (SEM) (error bars) of three independent experiments. The *p*-values were assessed using the two-tailed Student's *t*-test. A *p*-value below 0.05 was considered as significantly different (***$p < 0.005$; ** $p < 0.01$; * $p < 0.05$; n.s. (no significance), $p \geq 0.05$).

15. Accession numbers

The coordinates and structure factors for ChaC2, ChaC2 E74Q, and ChaC2 E83Q have been deposited in the Protein Data Bank with accession IDs, 6K95, 6KY0, and 6KY1, respectively.

III. Results

1. ChaC2 structure was determined through rational Met-substitution for MAD phasing

ChaC2 does not share a reasonably high sequence similarity to proteins with known structures, which hindered the MR for phasing. The subsequent multiple isomorphous replacement (MIR) method also failed to solve the phasing problem of the ChaC2 diffraction data set. In addition, ChaC2 contains only one Met residue at the N-terminus and the first Met was not sufficient to solve the phasing problem by MAD using SeMet-derivatized ChaC2 protein with 184 amino acid residues. To overcome this lack of anomalous signaling, the Met-substitution method was used [36, 47]. To this end, I initially chose the Leu and Ile residues located at the junction of two different secondary structure regions, which normally exhibited average or high predicted-solvent accessibility. Therefore, I used the *SABLE* server [36], which predicted the solvent accessibility bases on secondary structure of protein and suggested a number of potential residues to be replaced with Met (Figure 8). In order to further optimize the Met-substitution residues, we intensively investigated the amino acid sequence conservation among homologous ChaC2 proteins. Taken all together, I selected five residues: Leu21, Leu52, Leu119, Ile152, and Leu181, for Met-substitution (Figure 8). I attempted various combinations of Met-substitution with the five residues to produce single crystals for the structure determination of ChaC2. Eventually, I found that the ChaC2 mutant with L21M, L119M, and L181M yielded good diffracting-quality crystals, which allowed me to solve the crystal structure of ChaC2 at 2.8 Å resolution, using the MAD method. The data collection and structure refinement statistics are summarized in Table 1.

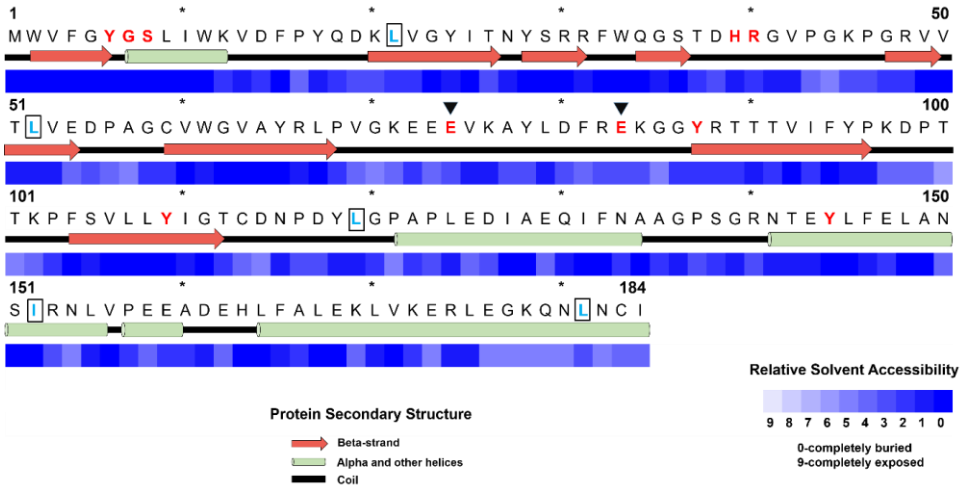

Figure 8. Secondary structure and solvent accessibility predictions using the *PSIPRED* and *SABLE* server.

The predicted helices, β-strands, and coils are shown in pale green, deep salmon, black, respectively, below the ChaC2 amino acid sequence. The residues predicted to be buried or exposed are denoted in a gradient of white to blue colors. The conserved key residues among the GGCT proteins are shown in red (see also Figure 14). Glu83 and Glu74 are indicated with black triangles. The residues substituted with Met in my study are colored in cyan and shown in black squares.

Table 4. Multi-wavelength anomalous diffraction phasing statistics

	SeMet-λ1 (peak)	SeMet-λ2 (edge)	SeMet-λ3 (remote)
Data collection			
Wavelength (Å)	0.9793	0.9795	0.9717
Space Group	$P3_121$		
Resolution (Å) *	50.00–2.80 (2.85–2.80)	50.00–2.95 (3.00–2.95)	50.00–3.05 (3.05–3.00)
R_{sym}*	0.130 (0.948)	0.130 (0.867)	0.148 (0.946)
Total no. observations	136,727	117,519	111,444
Total no. unique reflections	11,761	10,110	9,597
$I/\sigma(I)$ *	14.7 (3.1)	14.7 (3.1)	47.7 (3.5)
Completeness (%)*	99.9 (100.0)	99.9 (100.0)	99.9 (100.0)
Multiplicity*	11.6 (11.7)	11.6 (11.7)	11.6 (11.6)

*Values in parentheses correspond to highest-resolution shell.
X-ray diffraction experiment was performed at PAL–7A, Pohang Photon Factory
(Pohang, Korea).

After several rounds of iterative model building and refinement of the SeMet-derivatized ChaC2 structure, unexpected electron densities were found adjacent to the suggested active site cavity. Furthermore, the electron maps of the Val60–Asp80 region could not be well defined, despite the overall electron map quality of ChaC2 being excellent. With the native ChaC2 crystal structure at a higher resolution (2.3 Å), I was able to finally determine that these electron densities came from the loop region (residues Val60–Asp80) of the adjacent ChaC2 molecule. There were three ChaC2 molecules in an asymmetric unit (ASU) (Figure 9). Each ChaC2 molecule formed a domain-swapping homodimer with a ChaC2 molecule from the adjacent ASU (Figure 9). The R_{work} and R_{free} values for the ChaC2 structure were 0.23 and 0.28, respectively, which confirmed the structural reliability of ChaC2 with other parameters. The data collection and refinement statistics are summarized in Table 2.

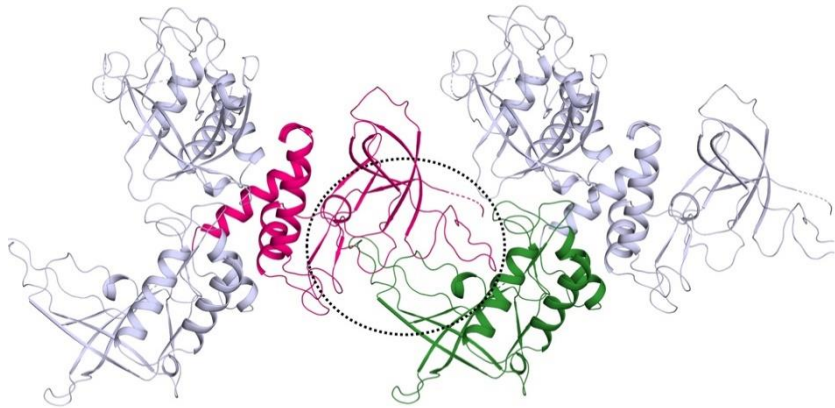

Figure 9. Schematic representation of ChaC2 molecules in the crystal.

ChaC2 molecules of homodimer from two ASU are colored in pink and green, respectively. The swapping-loop region is donated with a black dotted circle

Table 5. Data collection and refinement statistics of ChaC2 structures

	ChaC2 (PDB ID: 6K95)	ChaC2 E74Q (PDB ID: 6KYO)	ChaC2 E83Q (PDB ID: 6KY1)
Data collection			
Beam line	Spring–8	PAL–7A	PAL–5C
Wavelength (Å)	0.9000	0.9793	0.9795
Space Group	*C*2	$P3_1$	$P3_1$
Cell dimensions			
a, b, c (Å)	108.84, 62.16, 103.62	72.92, 72.92,104.25	72.64, 72.64, 104.13
α, ß, γ (°)	90.00, 90.01, 90.00	90.00, 90.00, 120.00	90.00, 90.00, 120.00
Resolution (Å)*	50.00–2.30 (2.34–2.30)	50.00–2.17 (2.21–2.17)	50.00–2.04 (2.08–2.04)
R_{sym}*	0.056 (0.403)	0.070 (0.480)	0.070 (0.563)
Total no. reflections	164,479	311,397	241,362
Total no. unique reflections	31,202	33,032	38,900
I/σ(I)*	23.0 (5.2)	24.5 (7.3)	42.5 (4.2)
Completeness (%)*	99.5 (99.9)	99.7 (99.9)	99.9 (100.0)
Multiplicity*	5.3 (5.2)	9.4 (9.5)	6.2 (6.0)
Refinement			
Resolution range (Å)	37.38–2.30	31.59–2.17	62.91–2.04
R_{work}/R_{free}†	0.234/0.287	0.221/0.257	0.227/0.255
No. atoms			
Protein	4,206	4,133	4,133
Water	17	77	127
Average B factors (Å^2)	73.00	21.37	35.22
Protein	39.36	21.37	29.50
Water	54.79	31.19	55.13
R.m.s. deviations			
Bond length (Å)	0.009	0.007	0.009
Bond angles (°)	1.121	1.412	1.300
Ramachandran Favored/outlier	98.6/0.0	99.1/0.0	96.8/0.0

*Values in parentheses are for the highest resolution shell.
†About 5% of the reflections were excluded from the refinement for R_{free} calculation.

2. The overall structure of ChaC2 adopts the GGCT fold

The ChaC2 structure exhibited a mixed α/β topology with nine β-strands (β1-β9), three α-helices (α1-α3), and two 3_{10}-helices (η1 and η2) (Figure 10A, 10B). The five β-strands β1, β2, β7, β8, and β9 form a central antiparallel β-sheet (β1↑β2↓β7↑β8↓β9↑). The connecting loop between β-strand β3 and β4 crosses over and twists around the corresponding loop between β-strand β6 and β5 (Figure 10A). In addition, the ChaC2 contains the conserved catalytic cavity that is observed among proteins containing the GGCT fold [11], and formed by the key ^{6}YGS^{8} motif in loop1 (residues Gly5-Arg30), Tyr87 and Tyr109 in β8 and β9, β1, Tyr144 in helix α2, and hydrophilic residues Asn34, His39, and Arg40 in the loop3 (residues Asn34-Gly46) (Figure 10A and Figure 8). As mentioned earlier, the ChaC2 structure exhibited a domain-swapping conformation with loop2 (residues Val60-Asp80), flipping out from the core domain (Figure 10A, 10B). Thus, the Glu residues, which are generally known as general acid/base catalytic residues in the GSH degradation reaction, were ambiguous in the activity cavity of one ChaC2 monomer (Figure 10A).

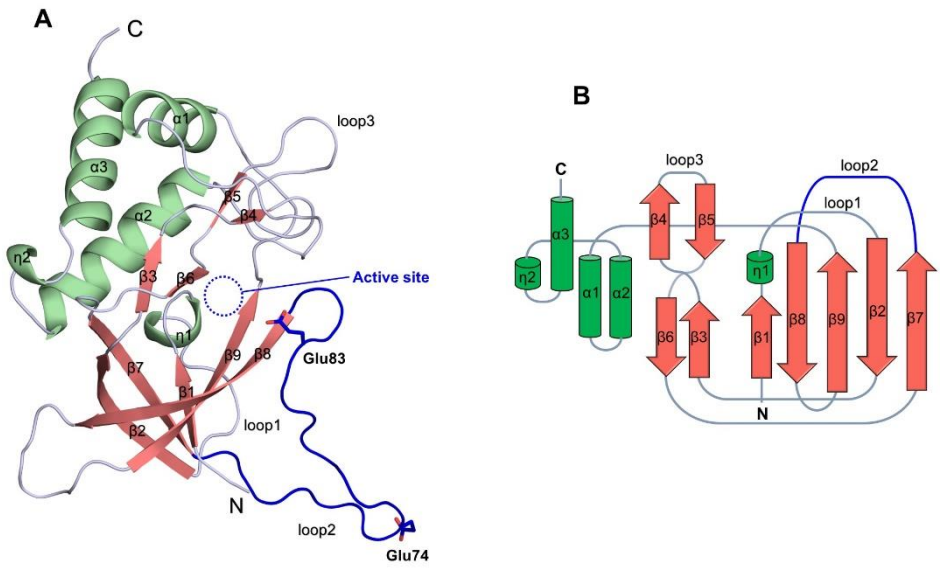

Figure 10. Overall structure of ChaC2

(A) Structure of ChaC2. Helices, β-strands, and loops are colored in green, salmon, and light blue, respectively. The active site of ChaC2 is donated with a blue dotted circle. Loop2 is colored in blue. The side chains of Glu74 and Glu83 are shown as stick models. (B) Topology diagram of ChaC2. The secondary structure elements are denoted as in (A).

3. Domain-swapping structure of the ChaC2 homodimer represents an open conformation.

In each ChaC2 molecule in ASU, the loop2 region protruded from the center crystallographic trimer and formed an unprecedented domain-swapping homodimer with the adjacent ChaC2 molecule, which I call an open conformation (Figure 11A). When I calculated the *mFo-DFc* map at 2σ, the loop2 region exhibited unambiguous positive electron densities that confirmed the domain-swapping ChaC2 homodimer (Figure 11A). Analysis of the oligomeric state of the ChaC2 structures using *PISA* web server [48] also indicated the formation of a stable homodimer with a relatively large buried area of 1349.4 $Å^2$, coverings 13.1% of the ChaC2 monomer surface area. The dimer interface included the loop2 region from one ChaC2 monomer and the loop1 from the other ChaC2 monomer (Figure 11A). Coincidently, the domain-swapping interface was located adjacent to the proposed active site cavity, which is characterized by loop1, α2, β8, and β9, as previously mentioned. In addition, the domain-swapping ChaC2 homodimer established stable interactions via numerous hydrogen bonds and salt bridge networks in the predicted active site cavity (Table 3). Furthermore, Lys12 and Arg40 from one ChaC2 monomer formed salt bridges with the side chain of Glu73 from the other ChaC2 monomer. In addition, 22 hydrogen bonds were tightly formed between Ser8/Lys12/Arg40/Tyr109/Tyr144 from one ChaC2 monomer and Lys71/Glu73/Glu74/Lys76 from the other ChaC2 monomer (Table 3 and Figure 11B). Notably, among these residues, Ser8, Arg40, Glu74, Tyr109, and Tyr144 were strictly conserved among the GGCT enzymes and contributed to the active site cavity (Figure 8 and Figure 14).

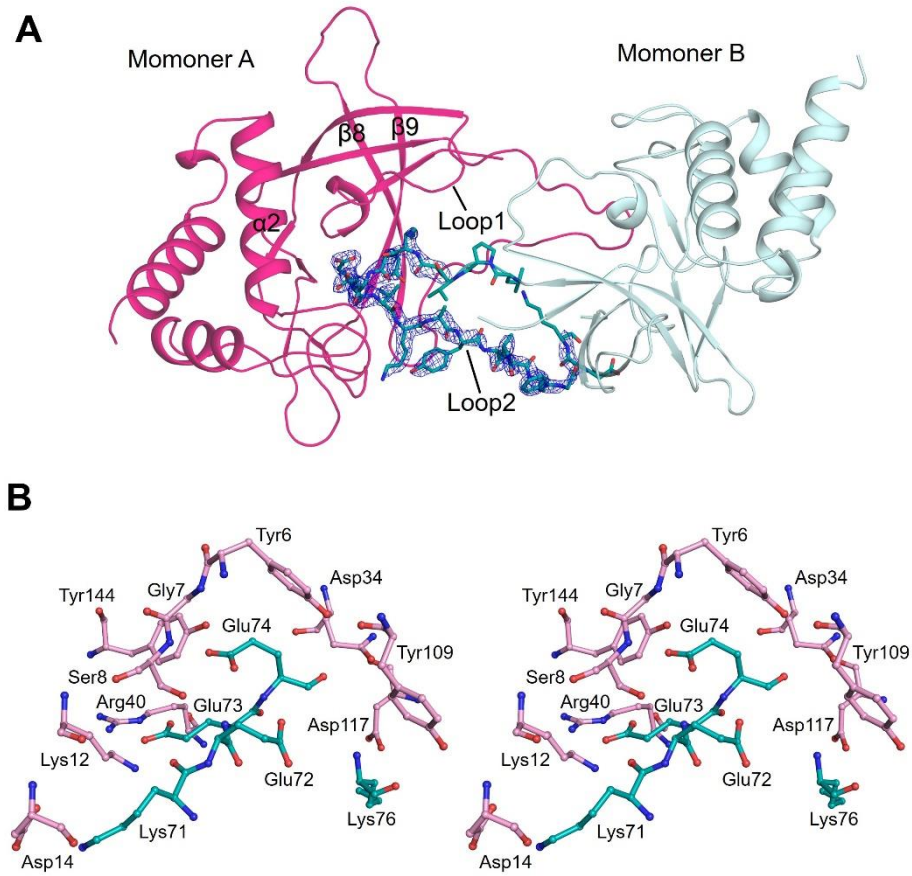

Figure 11. Domain swapping of ChaC2.

(A) Swapping-domain ChaC2 homodimer in the crystal structure. Two ChaC2 monomers are colored in pink and pale cyan, respectively. The loop2 residues are represented as green stick models and their *mFo-DFc* electron densities of 2.0σ are shown with blue meshes. (B) A stereo-view of the homodimeric interface of ChaC2. The residues from the two interacting ChaC2 molecules are denoted with pink and cyan models, respectively. The nitrogen and oxygen atoms are denoted in blue and red, respectively.

Table 6. Interaction between two molecules in ChaC2 domain-swapping homodimer by PISA web server

Hydrogen Bond			Salt Bridge Interaction		
Monomer A	Monomer B	Distance (Å)	Monomer A	Monomer B	Distance (Å)
Ser8 [N]	Glu74 [OE2]	2.80	Lys12 [NZ]	Glu73 [OE2]	2.57
Ser8 [OG]	Glu74 [OE1]	3.06	Arg40 [NE]	Glu73 [OE2]	3.51
Ser8 [OG]	Glu73 [N]	2.90	Arg40 [NE]	Glu73 [OE1]	2.60
Ser8 [OG]	Lys71 [O]	3.56	Arg40 [NH2]	Glu73 [OE2]	2.73
Arg40 [NE]	Glu73 [OE1]	2.60	Arg40 [NH2]	Glu73 [OE1]	3.43
Arg40 [NH2]	Glu32 [OE2]	3.73	Glu73 [OE2]	Lys12 [NZ]	2.57
Lys71 [NZ]	Ser8 [OG]	3.56	Glu73 [OE1]	Arg40 [NE]	2.60
Glu73 [N]	Ser8 [OG]	2.90	Glu73 [OE2]	Arg40 [NE]	3.51
Tyr109 [OH]	Lys76 [O]	3.35	Glu73 [OE1]	Arg40 [NH2]	3.51
Tyr144 [OH]	Glu74 [OE2]	2.30	Glu73 [OE2]	Arg40 [NH2]	3.43
Lys71 [O]	Ser8 [OG]	3.61	Lys71 [NZ]	Asp14 [OD1]	3.47
Glu74 [OE1]	Ser8 [OG]	3.06	Lys71 [NZ]	Asp14 [OD2]	3.53
Glu74 [OE2]	Tyr144 [OH]	2.60	Lys76 [NZ]	Asp117 [OD1]	3.78
Glu73 [OE1]	Arg40 [NE]	2.60	Lys76 [NZ]	Asp117 [OD2]	2.72
Glu73 [OE2]	Arg40 [NH2]	2.73	Asp14 [OD2]	Lys71 [NZ]	3.53
Asp117 [OD2]	Lys76 [NZ]	2.72	Asp14 [OD1]	Lys71 [NZ]	3.47
Ser8 [OG]	Glu73 [N]	2.90	Asp117 [OD2]	Lys76 [NZ]	2.72
Lys76 [O]	Tyr109 [OH]	3.35	Asp117 [OD1]	Lys76 [NZ]	3.78
Lys12 [NZ]	Lys71 [O]	3.10			
Lys12 [NZ]	Glu73 [OE2]	2.57			
Lys76 [NZ]	Asp117 [OD2]	2.49			
Glu73 [N]	Lys12 [NZ]	2.57			

4. Single mutations of E74Q and E83Q induced conformational changes in the domain-swapping ChaC2 homodimer and resulted in a closed conformation

Despite many attempts, I was unable to determine any complex structure of ChaC2 with the substrate GSH or the products 5-L-oxoproline and Cys-Gly in the GSH degradation reaction, which would have revealed the exact binding mode or snapshot of the catalytic mechanism. Nevertheless, structural similarity analyses implemented with the coordinates of ChaC2 using the *DALI* web server [49] demonstrated that the overall structure of ChaC2 shares a highly conserved scaffold with the other GGCT protein structures (Table 4). ChaC2 showed high structural similarities to yeast glutathione-specific gamma-glutamylcyclotransferase (PDB ID: 5HWI, z-score = 19.2, sequence identity = 38%), human GGCT (PDB ID: 2PN7, z-score = 12, sequence identity = 21%), and human GGACT (PDB ID: 3JUC, z-score = 7.2, sequence identity = 21%). When the structure of the domain-swapped ChaC2 homodimer was superimposed with the structurally similar enzymes, the Glu74 residue in loop2 of ChaC2 was found to be located at dimer interface and structurally equi-positional to other active-site Glu residues in the structurally similar enzymes [11-13] (Figure 12). Thus, I hypothesized that Glu74 plays a critical role not only in the catalytic function but also in domain-swapping dimerization.

Table 4. Structural similarity of ChaC2 to other known structures in PDB using Dali server

Proteins	Z-score	Sequence identity (%)	PDB IDs
Yeast glutathione-specific γ-glutamylcyclotransferase	19.2	38	5HWI
Human γ-glutamylcyclotransferase C7orf24	12.0	21	2PN7
Bacillus subtilis Ykqa protein	11.6	23	2QIK
Human hypothetical LOC79017 protein	11.4	21	2I5T
Arabidopsis thaliana AT5G39720.1 protein	7.7	17	2G0Q
Human γ-glutamylaminecyclotransferase	7.2	14	3JUC
Pyrococcus horikoshii uncharacterized PH0828 protein	6.9	16	1V30
Arabidopsis thaliana At3g28950.1 protein	6.6	19	2JQV
Kluyveromyces lactis allophanate hydrolase	6.1	9	4IST
Escherichia coli glutamyl-tRNA aminotransferase C4763	5.6	11	5C5Z
Escherichia coli hypothetical UPF0131 protein	5.4	23	1XHS
Structures with Z-scores > 5 were selected.			

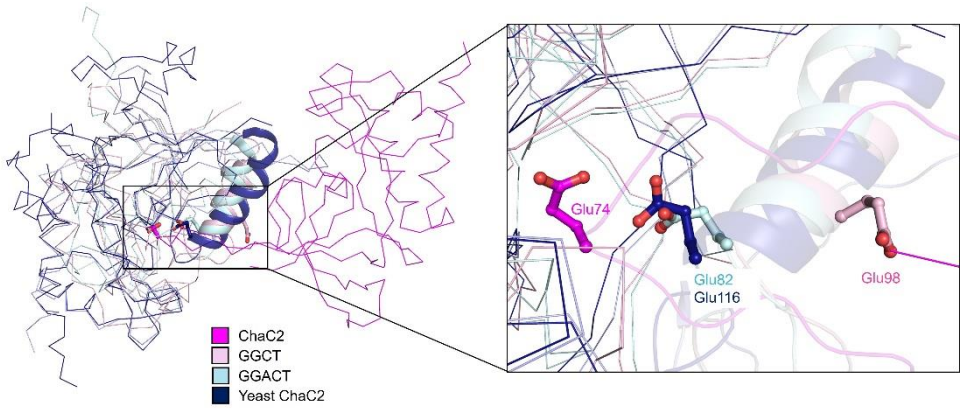

Figure 12. Structural superposition of the structures of human ChaC2, GGCT (PDB ID: 2PN7), GGACT (PDB ID: 3JUC), and yeast ChaC2 (PDB ID: 5HWI). Two human ChaC2 molecules in a crystallographic homodimer are colored in magenta and light blue, respectively. Human GGCT, GGACT, and yeast ChaC2 are colored in light pink, pale cyan, and blue, respectively. The Glu residues in the active site cavities of human ChaC2, GGCT, and GGACT and yeast ChaC2 are shown as stick models.

To validate my hypothesis, I generated a ChaC2 E74Q mutant and determined its crystal structure. The ChaC2 E74Q structure was solved at 2.2 Å resolution (Table 2), with one homo-trimer of ChaC2 E74Q A, B, and C in ASU (Figure 13A). Compared with the ChaC2 monomer in the domain-swapped dimer, ChaC2 E74Q A (B) adopted a helix conformation in the equivalent position of the ChaC2 loop2, which is mainly involved in domain-swapping (Figure 13A, B). The helix withdrew inward towards the center of a monomer molecule and did not form a domain-swapped homodimer, resulting in a closed conformation (Figure 13B). The Gln74 withdrew from the adjacent active site cavity then protruded outward towards the rear of the newly formed helix (Figure 13B). Interestingly, neither the loop2 nor the helix conformation was not visible in the equivalent region of ChaC2 E74Q C despite the overall fold of ChaC2 E74Q C being identical to that of the ChaC2 monomer (Figure 13A). This finding suggests that ChaC2 E74Q C is a snapshot of a transition from a loop conformation to a helix.

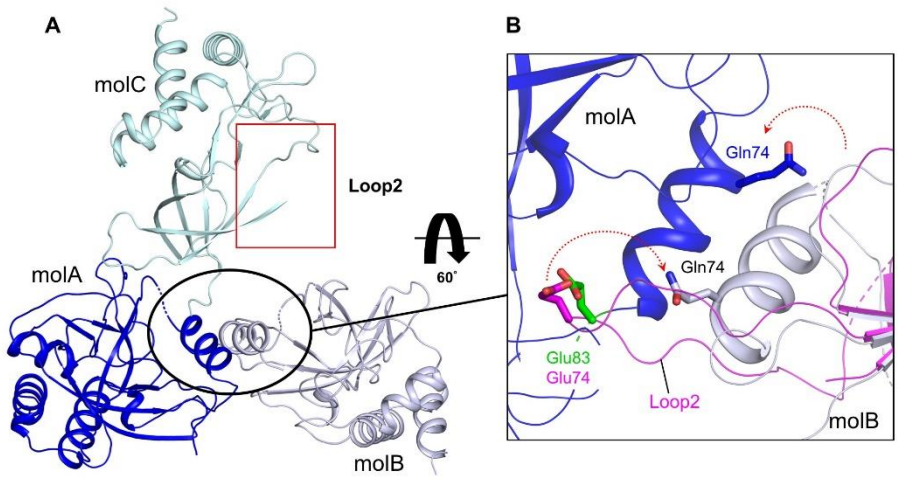

Figure 13. Conformation changes of ChaC2 E74Q and ChaC2 E83Q mutants. (**A**) Structures of ChaC2 E74Q mutant. Three ChaC2 E74Q molecules (mol) in an ASU are denoted in blue (molA), white blue (molB), and pale cyan (molC), respectively. The loop2 region of molC is marked in red circle. (**B**) Newly formed helices on the interface of ChaC2 E74Q molA and molB superimpose to loop2 region of ChaC2 monomer. Side chains of Gln74 and Glu83 of ChaC2 E74Q molA and molB are represented as stick models. The Glu83 of ChaC2 E74Q molA and Glu74 of ChaC2 monomer are colored in green and magenta, respectively. The Gln74 of ChaC2 E74Q molA and molB are colored in blue and white blue, respectively

Surprisingly, the ChaC2 E74Q A structure was found to have Glu83 also move along with the newly formed helix, to become located at the active site cavity of ChaC2 E74Q A (B) (Figure 13B). The Glu83 replaced the Glu74 and extended into the active site cavity of the new helix conformation monomer (Figure 13B). As a result, Glu83 aligned very well with other catalytic Glu residues of GGCT enzymes and with Glu74 in the domain-swapping ChaC2 homodimer (Figure 13B and Figure 19). Furthermore, my amino acid alignment showed that Glu83 was strictly conserved with other catalytic residues of yeast ChaC2, human GGCT, human GGACT, and human ChaC1 (Figure 14). Therefore, I decided to investigate the function of Glu83 in greater detail. I generated a ChaC2 E83Q mutant and determined its crystal structure. The ChaC2 E83Q structure was solved at 2.0 Å resolution. The overall fold of the ChaC2 E83Q molecules, A and C, resembled those of ChaC2 E74Q, A and C, respectively (Figure 15). The loop1 regions in both ChaC2 E83Q and ChaC2 E74Q were slightly rotated compared with that of ChaC2 (Figure 15, right panel). Noticeably, the electron density around the loop2 region of the ChaC2 E83Q C molecule was more clearly than that of the ChaC2 E74Q C molecule (Figure 16), supporting that there is an existing partial-changing conformation, wherein loop1 seems to be involved in the mobility of loop2 during conformational switching.

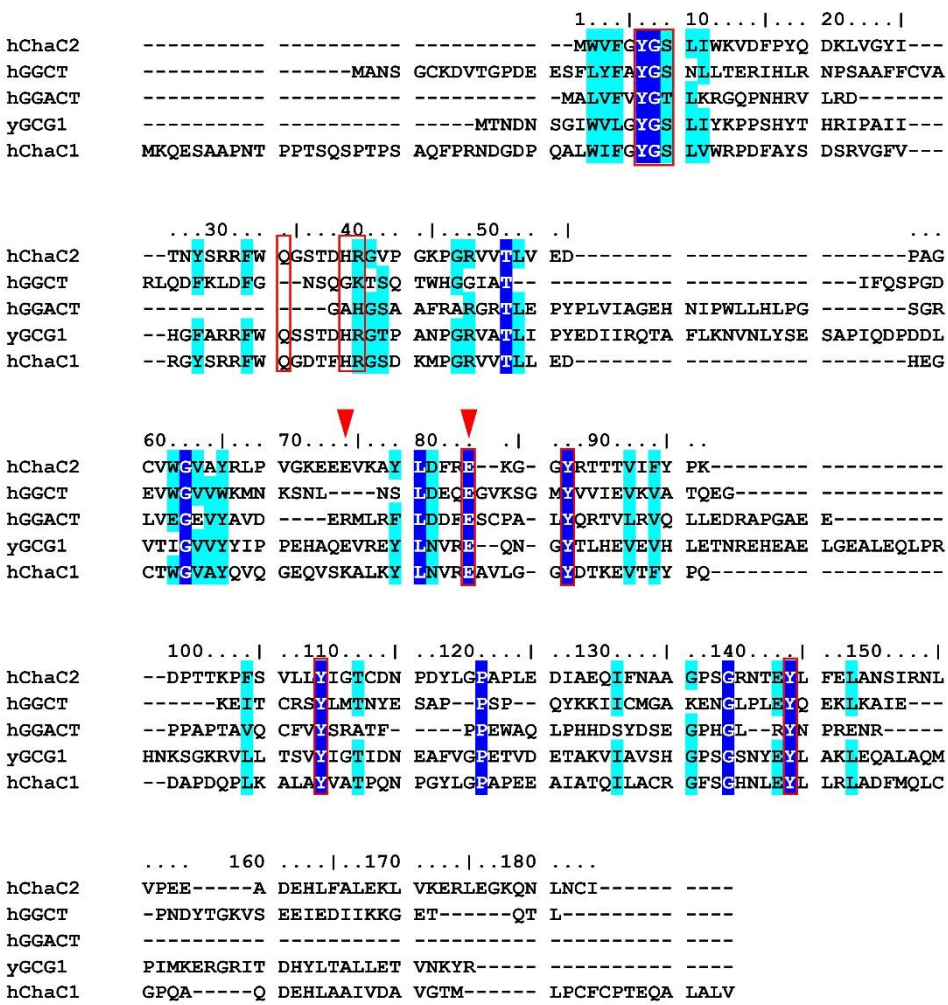

Figure 14. Sequence alignment of GGCT proteins

ChaC2 (UniProt ID: Q8WUX2) and four representative GGCT proteins: human GGCT (UniProt ID: 075223), human GGACT (UniProt ID: Q9BVM4), yeast GCG1 (UniProt ID: P32656), and human ChaC1 (UniProt ID: Q9BUX1). Among these five proteins, the identical/similar residues are shaded in blue/cyan, respectively. The residues involved in GSH binding are additionally boxed in red square. The Glu74 and Glu83 of human ChaC2 are indicated with red triangles. The alignment was performed by Clustal Omega software with ESPRIPT3.

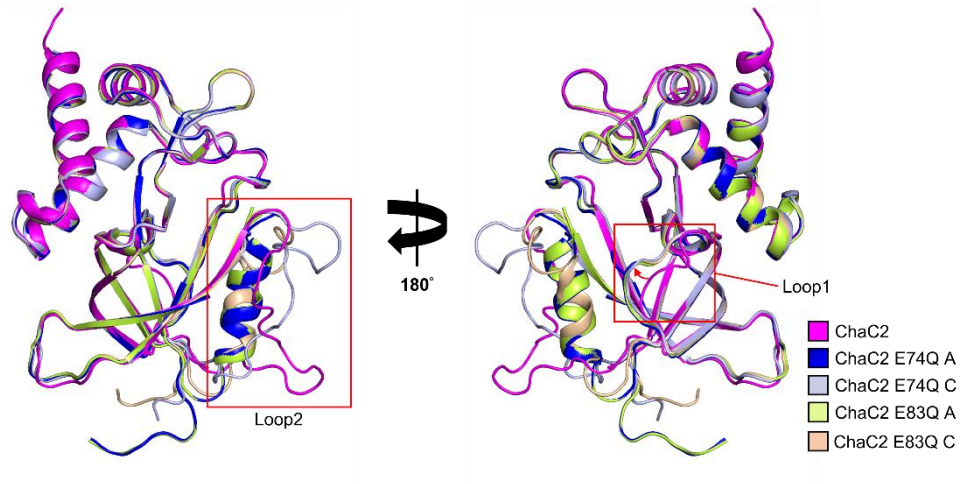

Figure 15. Superimposition of ChaC2 and its mutants.

The structure of ChaC2 (magenta), ChaC2 E74Q (blue and light blue), and ChaC2 E83Q (green and wheat) showing the different conformations of loop2 (left) and loop1 (right) are superimposed. Loop2 and loop1 are donated with red boxes

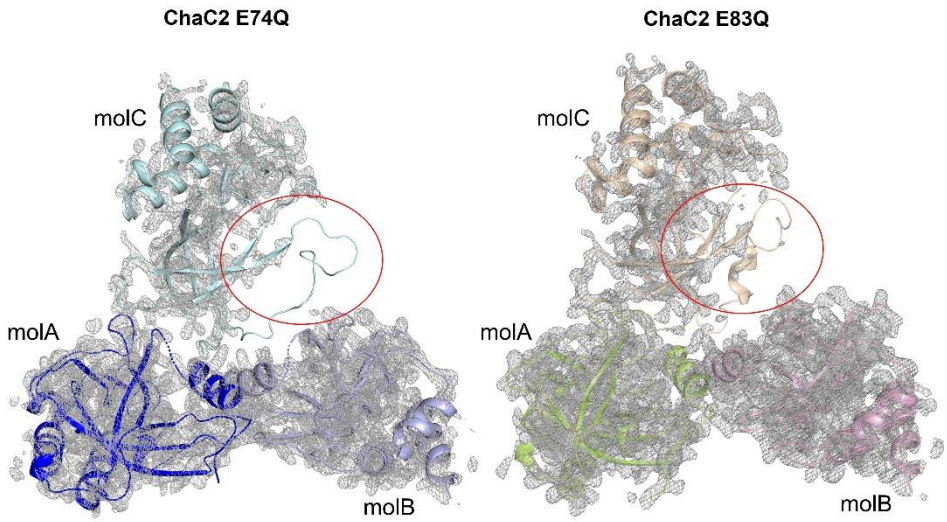

Figure 16. *mFo-DFc* electron densities of ChaC2 E74Q (left) and ChaC2 E83Q (right) contoured at 2.0σ.

The loop2 regions of ChaC2 E74Q and ChaC2 E83Q are indicated with red circles.

To validate the oligomeric state of ChaC2 in solution, I implemented size-exclusion chromatography followed by SDS-PAGE and native-PAGE analyses. The elution profile of ChaC2 showed a major peak corresponding to the monomer status, and the eluted proteins generated a single monomer band in SDS-PAGE and native-PAGE gels (Figure 17). Interestingly, the protein band of the ChaC2 sample from the major peak was also distributed in discrete bands above the major band in native-PAGE, implying that there exist ChaC2 molecules in a higher oligomeric state. (Figure 17, left panel). In the cases of ChaC2 E74Q and ChaC2 E83Q, the elution profiles from size-exclusion chromatography also showed a monomer peak, and the mutants of ChaC2 exhibited a single monomer band in SDS-PAGE and native-PAGE gels (Figure 17, middle and right panels, respectively). These data indicate that ChaC2 could interact together and adopt higher oligomeric states, whereas ChaC2 E74Q or ChaC2 E83Q may exist as monomers in solution, which further supports the crystal structure of the domain-swapping ChaC2 homodimer and ChaC2 E74Q and ChaC2 E83Q monomers.

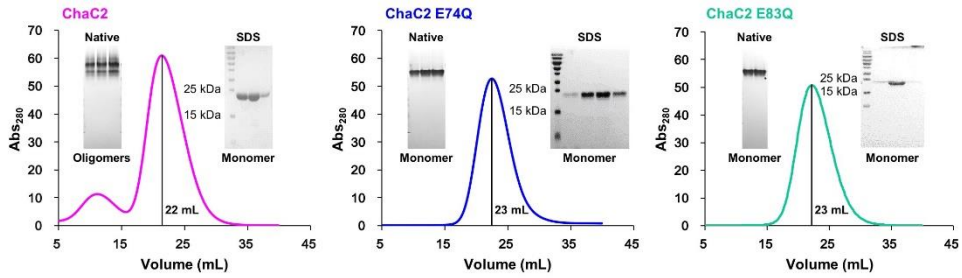

Figure 17. Size-exclusion chromatogram for ChaC2 (pink line), ChaC2 E74Q (blue line), and ChaC2 E83Q (green line).

The SDS-PAGE and native-PAGE gel of the main peak protein fractions are shown beside the chromatograms.

5. Structural comparison of human ChaC2 and other GGCT enzymes reveals flexibility in the domain-swapping region

Despite sharing the conserved β-barrel fold where the substrate ɣ-glutamyl moiety binds, each GGCT protein contains a different number of appended α-helices, β-strands, and loops around the β-barrel topology to recognize substrates specifically [11-13]. The L-ɣ-glutamyl moiety of GGCT links to L-α-amino acids, but that of GGACT links to extended alkylamines [12]. In order to elucidate the structure-based GSH specific activity information, I compared the crystal structure of ChaC2 with other GGCT structures. ChaC2 exhibited remarkable structural differences in the loop2 and loop1 regions that lie in the active site, compared with GGCT and GGACT (Figure 18). The loop2 region in the ChaC2 structure was involved in the domain-swapping dimer with loop1 of the adjacent ChaC2, while the loop2 regions of ChaC2 E74Q and other GGCT proteins adopted a helical conformation (Figure 18). Consequently, the active site cavity of ChaC2 was relatively flexible, compared with other structurally homologous enzymes.

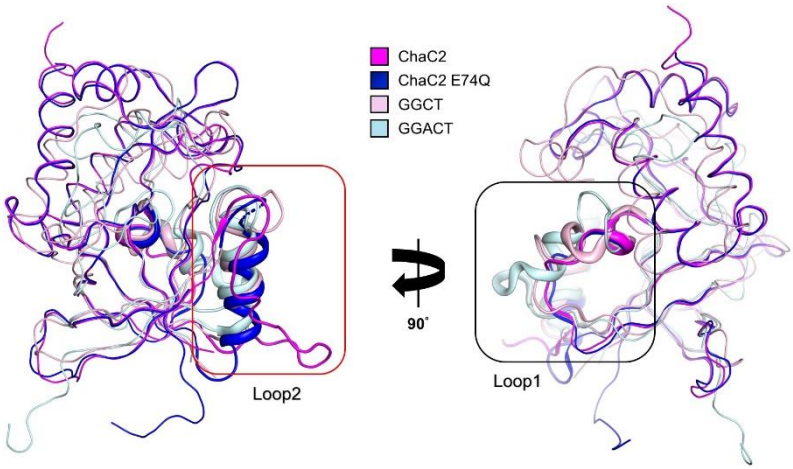

Figure 18. Structural comparison of human ChaC2, human GGCT, and human GGACT.

The structures of ChaC2 (magenta), ChaC2 E74Q (blue), GGCT (PDB ID: 2RBH, pink), and GGACT (PDB ID: 3JUC, cyan) are superimposed. The loop2 and loop1 regions of ChaC2 are donated by red (left) and black (right) boxes, respectively

The GGCT proteins generally have an acid/base Glu in their active site; Glu98 (in human GGCT) [12], Glu82 (in human GGACT) [13], and Glu116 (yeast ChaC2) [11] (Figure 12). To identify the equivalent catalytic Glu residue of ChaC2, I carefully investigated the active site residues of ChaC2 with other GGCT enzymes (Figure 19). The superimposition of their structures clearly revealed that Tyr6, Gly7, Ser8, His39, Tyr87, Tyr109, and Tyr144 of ChaC2 were strictly conserved with other GGCT enzymes (Figure 19). Interestingly, the catalytic Glu was aligned very well with both the Glu74 and Glu83 of ChaC2 and ChaC2 E74Q, respectively. Thus, I propose that ChaC2 has two alterative acid/base Glu residues, corresponding to two state conformations.

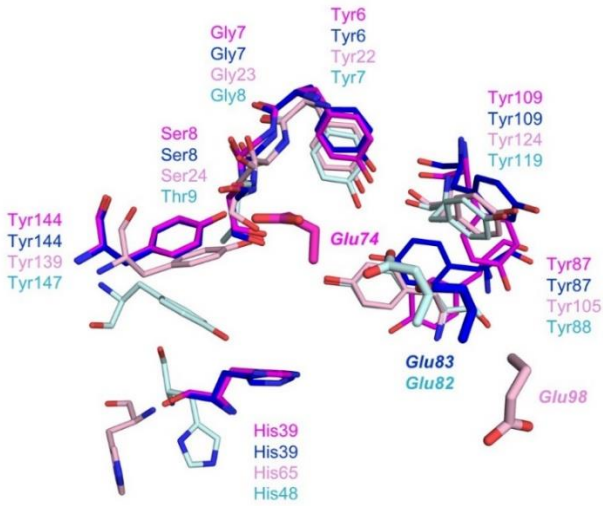

Figure 19. Substrate-binding residue comparison of human ChaC2, ChaC2 E74Q, human GGCT, and human GGACT.

The substrate-binding residues of GGCT and GGACT are denoted as pink and cyan stick models, respectively. ChaC2/ChaC2 E74Q residues overlapped with the substrate-binding residues of GGCT and GGACT are denoted as magnetic/blue stick models.

6. Purified ChaC proteins have GGCT activity in vitro

To confirm the GGCT activity of ChaC enzyme, I analyzed product after the GSH degradation reaction by LC-MS/MS as described in the Material and Methods. The results showed that the generation of 5-L-oxoproline after reaction because GSH is cleaved by ChaC enzymes. I also could observe the 5-L-oxoproline level after reaction of ChaC1 enzyme much higher than that of ChaC2, indicating that ChaC1 has higher activity than ChaC2 (Figure 20)

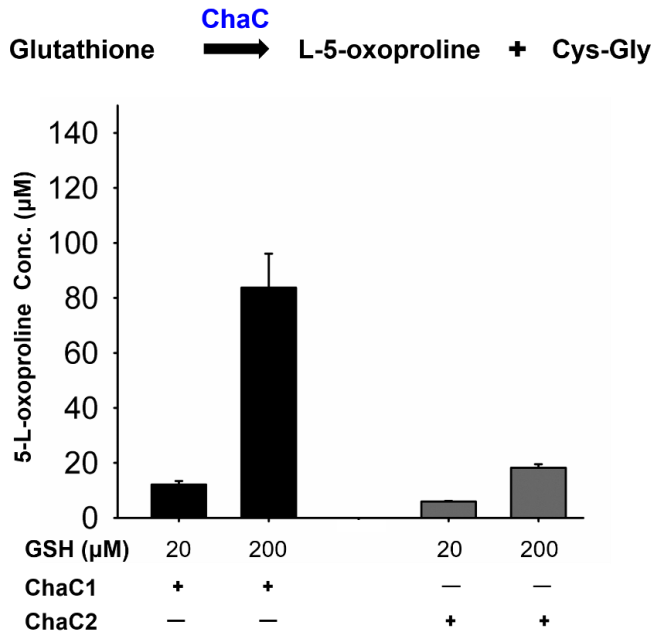

Figure 20. GSH degradation activity of ChaC enzyme.

L-5-oxoproline level increase after GSH degradation reaction with 1 μM of ChaC1 and ChaC2.

7. ChaC2 E74Q and ChaC2 E83Q mutation significantly reduced GSH-degradation activities in cell and in vitro.

Recent studies have shown that the overexpression of ChaC2 decreases the GSH levels in yeast cells [13] and gastric cancer cells [28]. To further elucidate the functional importance of Glu74 and Glu83, which I have analyzed structurally analyses respect to the domain-swapping and active site identification, I measured the GSH levels in ChaC2-, ChaC2 E74Q-, and ChaC2 E83Q-overexpressing HEK293 cells. ChaC2-overexpressing HEK293 cells showed lower GSH levels than control plasmid-overexpressing HEK293 cells (Mock) (Figure 21A), while ChaC2 E74Q- and ChaC2 E83Q-overexpressing HEK293 cells exhibited higher GSH levels than ChaC2-overexpressing cells (Figure 21A). The overexpression efficiency of exogenous ChaC2 proteins was verified by western blotting (Figure 21C).

I also implemented *in vitro* enzymatic assays to compare the GSH degradation activity of ChaC2, ChaC2 E74Q, and ChaC2 E83Q with human ChaC1 as a positive control. After 1 h of reaction, ChaC1 degraded 99.14% of the total GSH, however, ChaC2 was unable to degrade GSH as efficiently as ChaC1. ChaC2 was only able to degrade 58.97% the total GSH (Figure 21B), which is consistent with the previously reported results [10, 13]. ChaC2 E74Q and ChaC2 E83Q exhibited lower GSH degradation activity than ChaC2, that is, 21.34% and 27.15% degradation of the total GSH, respectively (Figure 21B). In summary, my GSH degradation assay demonstrated that human ChaC2 significantly reduced the GSH levels in cells and *in vitro*, and that both Glu74 and Glu83 residues play important roles in GSH degradation mediated by ChaC2. In conclusion, ChaC2 has GGCT activity and both Glu74 and Glu83 residues are involved not only in the structural conformation but also in the activity of ChaC2 in cells and *in vitro.*

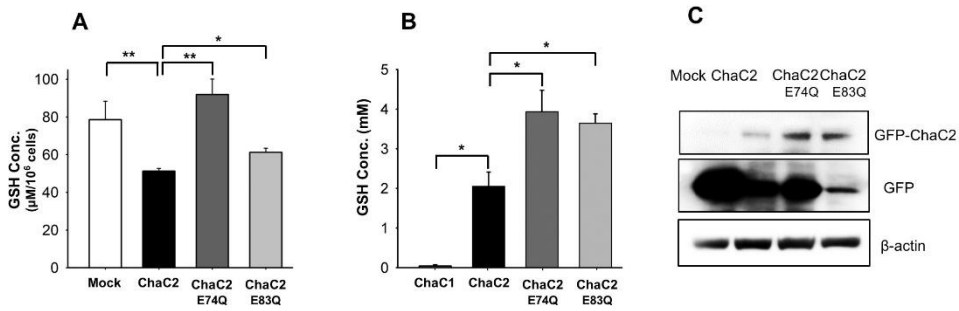

Figure 21. GSH level reduction in cells and *in vitro* by ChaC2.

(A) The GSH levels in HEK293 cells transfected with Mock, ChaC2, ChaC2 E74Q, and ChaC2 E83Q-containing pEGFP-C3 plasmids were measured. (B) Briefly, 5 mM of GSH was incubated with ChaC1, ChaC2, ChaC2 E74Q, and ChaC2 E83Q and the levels of residual GSH were measured. Data represent the mean ± SEM (error bars) of three independent experiments. Asterisks indicate statistically significant differences; * $p < 0.05$; ** $p < 0.01$. (C) Overexpression of ChaC2 in ChaC2-transiently transfected HEK293 cells. The cell lysates of the Mock, ChaC2, ChaC2 E74Q, and ChaC2 E83Q-transfected cells were analyzed by western blotting using a GFP antibody to detect GFP-tagged ChaC2 proteins.

8. ChaC2 overexpression promotes cell proliferation in MCF-7 breast cancer cell line

Recently, it has been reported that the downregulation of GGCT elicits an anti-proliferative effect in some cancer cell lines, such as breast cancer cell lines MCF-7, MCF-7/ADR, and MDA-MB-231 [50-52]. Interestingly, ChaC1 was suggested as a novel biomarker, since the overexpression of mammalian ChaC1 and its related transcript variants has been previously found to promote cell proliferation in breast cancer cell lines Hs578T and BT-20 [25, 53, 54]. When we analyzed the ChaC2 gene expression in breast cancer tissues from the online clinical database Oncomine, the TCGA, Turashvili Breast, and Karnoub Breast database showed that the transcriptional level of ChaC2 in invasive ductal breast carcinoma was significantly higher than in normal cells. In detail, the TCGA Breast source of ChaC2 (Reporter ID: A_23_P28571) reveals that when comparing 389 invasive ductal carcinomas to 61 breast samples, ChaC2 shows a 1.3 fold change in expression. The Turashvili Breast source of ChaC2 (Reporter ID: 235117_at) and Karnoub Breast source of ChaC2 (Reporter ID: 235117_at) also reveal that the ChaC2 gene expression fold changes were 4.5 and 1.8, respectively. In addition, the Kaplan–Meier plot of ChaC2 (Affymetric ID: 235117_at), according to gene overexpression in breast cancer patients and their overall survival information, showed that the survival rate of patients with breast cancer with high ChaC2 expression levels was significantly lower than that with low ChaC2 expression levels ($p < 0.001$) (Figure 22A). Notably, ChaC2 shares a high structural similarity with GGCT enzymes and a high amino acid sequence similarity with ChaC1. Based on these finding, I became interested in the biological effects of ChaC2 on breast cancer cells and related mechanisms. As such, I examined the effects of ChaC2 and ChaC2 active-site mutants (ChaC2 E74Q and ChaC2 E83Q) overexpressed in invasive ductal breast carcinoma MCF-7 cell line on cell growth by 3-(4,5-dimethylthiazol-2-yl)-2,5-diphenyltetrazolium bromide (MTT) assays and colony-forming assays. At the same protein level overexpression,

ChaC2 overexpression led to a significant increase in cell proliferation, compared to the Mock control (Figure 22B). However, ChaC2 E74Q overexpression did not induce cell proliferation as in ChaC2 overexpression, while ChaC2 E83Q overexpression elicited a similar cell proliferation level as ChaC2 overexpression (Figure 22B).

To confirm the MTT assay results, I further implemented a colony-forming assay with ChaC2-overexpressing MCF-7 cell line. After two weeks of transfection, I counted the ChaC2-overexpressing cell colony number and compared it with that of Mock treated-cells. Consistent with my MTT assay results, ChaC2-overexpressing cells formed more colonies than Mock treated-cells (Figure 22C, D). ChaC2 E74Q- and ChaC2 E83Q-overexpressing cells formed significantly less colonies than ChaC2-overexpressing cells (Figure 22D). The overexpression efficiency of the exogenous proteins after transiently transfecting ChaC2 and the Mock control into MCF-7 cells was evaluated by western blotting (Figure 22E). The results showed a significant overexpression of ChaC2 in this breast cancer cell line and confirmed that the ChaC2 mutants had similar expression levels as ChaC2 (Figure 22E). Taken together, the ChaC2 mutant data suggest that ChaC2 promotes breast cancer cell proliferation, while its active site mutants reduce this effect. As such, the GSH degradation activity of ChaC2 was shown to regulate the growth of MCF-7 breast cancer cell line. This will be discussed later in the discussion.

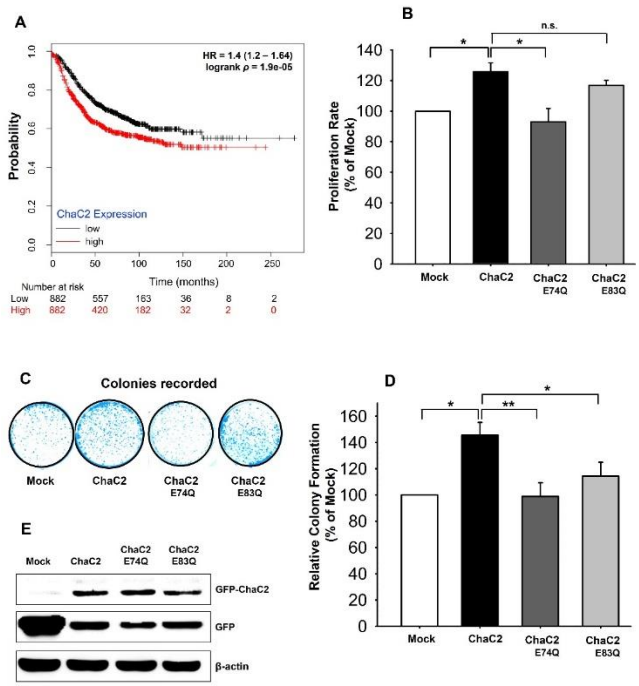

Figure 22. Proliferation of breast cancer cell lines by ChaC2 overexpression. (**A**) The Kaplan-Meier plots according to ChaC2 expression levels in patients with breast cancer. The plots show lower survival rates in patients with high ChaC2 expression compared to low ChaC2 expression. (**B**) Viability of ChaC2-overexpressed MCF-7 cell line was measured by MTT assay. The proliferation rate of cells is shown with relative percentages compared to the Mock-transfected cells. Data represent the mean ±SEM (error bars) of three independent experiments. Asterisks indicate statistically significant differences; * $p < 0.05$; ** $p < 0.01$. (C, D) Colony forming assay with ChaC2-overexpressed MCF-7 cell line. The representative photos were taken after 2 weeks from initial seeding (**C**). The relative percentages of the colony numbers of the ChaC2, ChaC2 E74Q, and ChaC2 E83Q-transfected cells to Mock-transfected cells are represented as the mean ± SEM (error bars) of three independent experiments (**D**). (**E**) The overexpression of ChaC2 in the ChaC2-transiently transfected MCF-7 cell line. Cell lysates of the Mock, ChaC2, ChaC2 E74Q, and ChaC2 E83Q-transfected cells were analyzed by western blotting using a GFP antibody to detect GFP-tagged ChaC2 proteins.

IV. Discussion

1. Role of domain-swapped ChaC2 homodimer conformation and its effects on catalysis

The overall structure of ChaC2 and its active site cavity are very similar to previously determined structures of GGCT enzymes. However, ChaC2 adopted a unique quaternary structure wherein two ChaC2 monomers exchanged their loop1 and loop2 structures to form a domain-swapped homodimer ChaC2, resulting in a more flexible and open active site cavity. It has been previously reported that the swapping loop of the HRAS-like tumor suppressor 3 (HRASLS) enzyme structure would be flexible or disordered without a bound ligand, and is involved in the re-arrangements to shield the active site from water molecules during the catalytic reaction steps [56]. According to the earlier structural study of yeast ChaC2, a similar short loop was also observed and suggested to change its conformation upon ligand binding, contributing to enhanced enzyme specificity [13]. To my surprise, the ChaC2 E74Q and ChaC2 E83Q mutants not only caused structural rearrangements but had an effect on the enzymatic function *in vitro* and *in vivo,* compared to the ChaC2 wild type. However, the ChaC2 E74Q and ChaC2 E83Q mutants did not abolish the GSH degradation activity, while the equivalent Glu residue mutations of ChaC1 and GGCT resulted in the complete loss of this activity [11, 15]. Collectively, my ChaC2 structures provide valuable insight into the mechanism by which the flexibility of the swapped loop regulates catalytic activities and maintains a constant GSH degradation rate. To initiate the catalysis, ChaC2 needs to undergo a conformational change in the flexible loop region, which allows and aids for the synchronous movement of the substrate inside and outside of the active sites. On the other hand, the swapped loop may also block the binding of substrates to ChaC2 and thereby limit the GSH degradation capacity of ChaC2. Therefore, the movement caused of swapped loop would be closely accompanied the steady and constant GSH degradation activity of ChaC2 in GSH metabolism.

The ChaC family belongs to the GGCT family but exclusively mediates the degradation GSH [13, 15]. Although the catalytic cavity of ChaC2 is generally conserved among other GGCT enzymes, the swapped loop and dimeric state have not been observed in the cavity of any GGCT enzyme. When the oligomeric states of ChaC1 and ChaC2 were compared using size-exclusion chromatography, ChaC2 mainly existed as a monomer in solution, while ChaC1 existed not only as a dimer but also as a tetramer (Figure 23). In addition, ChaC2 is constitutively expressed, exhibits lower activity, in the "housekeeping" GSH metabolism, while ChaC1 is only expressed in response to specific stresses or in tumors. These observations reinforce the notion that dimerization may be an important determinant in the regulation ChaC enzyme activity and substrate specificity. ChaC enzymes form dimer or higher oligomers for enzymatic functions in stressful or tumor conditions for enzyme crowding. The lower activity of ChaC2 compared to ChaC1 may be partly caused by domain-swapped dimerization, which further results in dimer/monomer equilibrium and open/closed conformation of the active site according to the oligomeric status.

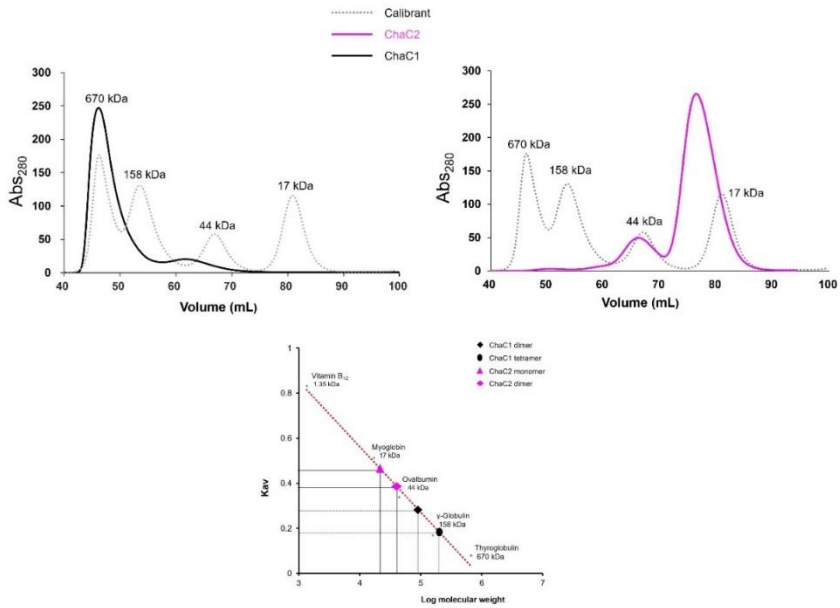

Figure 23. The oligomeric status of human ChaC1 and ChaC2.

The oligomeric status of human ChaC1 (26 kDa) and ChaC2 (20 kDa). The size-exclusion chromatograms of ChaC1 (left) and ChaC2 (right) are shown. ChaC1 and ChaC2 were loaded onto a HiLoad 16/600 Superdex 75 pg column at a flow rate of 1 mL/min. The eluted proteins were monitored at 280 nm. The chromatograms of ChaC1 and ChaC2 are indicated in black and magenta, respectively. The chromatogram of calibration mixture (thyroglobulin 670 kDa, ɣ-globulin 158 kDa, ovalbumin 44 kDa, and myoglobin 17 kDa) are shown in gray. The calibration/selectivity plot for standard proteins and ChaC2 proteins is shown in the panel below.

My structural analyses of the domain-swapped ChaC2 homodimer reveal a novel structural feature of the GGCT protein, which provides valuable insights regarding the contribution of unique swapped-domain arrangements for modulating enzyme activity. In addition, the domain-swapped conformation provides the first structural snapshot of the dynamic flexibility during the GSH degradation reaction mediated by ChaC2. I believe that the domain-swapped homodimer conformation plays a specific and efficient role in GSH degradation. To further validate the importance of the oligomeric status of ChaC2 in GSH degradation, the simulation of the molecular dynamics of the monomer/dimer transition in the presence or absence of GSH would be helpful.

2. Proposed mechanism of substrate recognition and GSH degradation of ChaC2

Although the conserved Glu83 residue is located far away from the interface of the swapped-loop homodimer, the ChaC2 E83Q mutation induced a conformational change, however, it did not significantly reduce the enzymatic activity, compared with the ChaC2 E74Q mutation. In the case of other swapped-loop structures, such as CD2 [57] and Suc1 proteins [58], mutations in residues distant from the hinge loop, which result in drastic monomer-dimer transitions, have been also observed. Considering that the ChaC2 E74Q and ChaC2 E83Q structures adopted a helical conformation in the domain-swapped region similar to the structure of GGACT in complex with 5-L-oxoproline [12] (Figure 24), Glu83 is likely to play an important role in domain-swapping and serve as an alternative catalytic residue. Furthermore, domain-swapped proteins are often considered as an open conformation, and, upon substrate- or ligand-binding, elicits conformational changes, resulting in a closed conformation [59]. Therefore, there is a good possibility that ChaC2 would switch its conformational status at the early stage of substrate GSH binding with the aid of the flexible loop region to bring the activity site residues in close proximity to GSH. The ChaC2 E74Q

and ChaC2 E83Q structures would be reminiscent of a closed conformation. To further elucidate the catalytic mechanism and the interaction mode between ChaC2 and GSH or 5-L-oxoproline (a product of the GSH degradation reaction by ChaC enzyme [15]), I generated ChaC2 E74Q and ChaC2 E83Q mutants in order to obtain their substrate or product complex. I attempted to determine the structure of ChaC2 E74Q or ChaC2 E83Q mutant in complexes with GSH or 5-L-oxoproline, but failed. As an alternative, I conducted simulated docking experiments and SPR experiments. I used the ChaC2 E74Q structure for the docking study, since the ChaC2 E74Q mutant still retains the GSH degradation activity of ChaC2, and the Glu83 residue in the ChaC2 E74Q mutant structure may act as an alternative active site, as in the aforementioned observations. To validate the docking program *Autodock Vina*, I implemented a control docking experiment with 5-L-oxorproline in the GGACT complex structure (PDB ID: 3JUC). 5-L-oxorproline was predicted to dock into the active site of GGACT as in the actual complex structure with a binding energy of – 5.1 kcal/mol (Figure 24). The docking results predicted that GSH or 5-L-oxorproline would bind to ChaC2 in very similar mode to that of the GGACT-5-L-oxorproline complex structure (Figure 25A). In the docking model, GSH or 5-L-oxorproline are recognized/stabilized by conserved active site residues Tyr6, Gly7, Ser8, Glu34, His39, Arg40, Tyr87, Tyr109, and Tyr144 of ChaC2, which also played similar roles in the GGACT-5-L-oxoproline complex structure (Figure 25B and Figure 19). In addition, the binding energies of GSH (– 6.3 kcal/mol) was lower than that of 5-L-oxoproline (– 5.2 kcal/mol), which suggests that GSH exhibits a higher binding affinity to ChaC2 than 5-L-oxoproline. We next examined the binding affinity of GSH and 5-L-oxoproline with ChaC2 by SPR. The SPR results showed that there is an interaction between GSH and ChaC2. Meanwhile, the interaction of 5-L-oxoproline with ChaC2 seemed too weak to be analyzed by SPR. Interestingly, ChaC2, ChaC2 E74Q, and ChaC2 E83Q showed a low binding response to GSH, whereas the ChaC2 E74Q E83Q showed a significantly high binding affinity with the calculated K_D value of 2.7 μM (Figure 25C).

The docking and SPR results imply that ChaC2 binds to GSH and the binding is instantaneous, and the release of product 5-L-oxoproline during the GSH degradation reaction is rapid. Furthermore, the mutation of active-site residues strongly bind to GSH and would inhibit the GSH degradation activity, resulting in higher binding affinity.

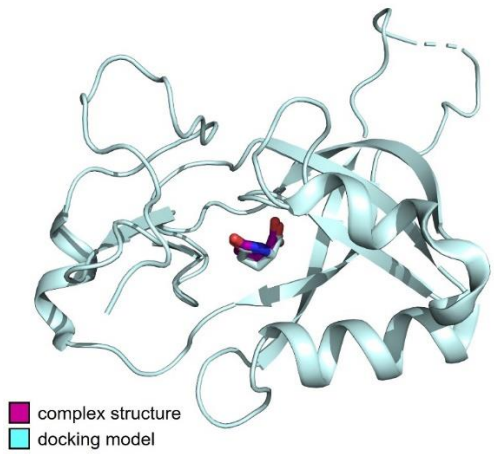

Figure 24. The control docking experiment result of the human GGACT with 5-L-oxoproline complex.

The 5-L-oxoprolines in the complex structure and docking model are shown as purple and cyan stick models, respectively. Oxygen atoms are denoted in red.

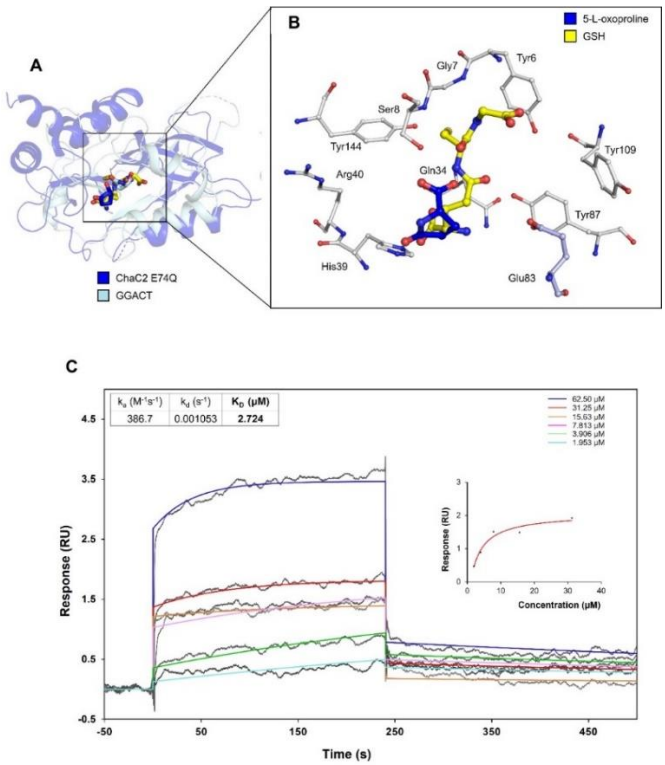

Figure 25. Binding assays of ChaC2 with GSH and 5-L-oxoproline.

(A) The docking models of GSH-ChaC2 E74Q and 5-l-oxoproline-ChaC2 E74Q have been superimposed onto the structure of GGACT in complex with 5-l-oxoproline. ChaC2 E74Q and GGACT are colored in blue and pale cyan, respectively. The GSH (docked into ChaC2 E74Q), 5-l-oxoproline (docked into ChaC2 E74Q), and 5-l-oxoproline (bound to GGACT) are denoted as yellow, blue, and pale cyan stick models, respectively. The docking binding energies of GSH and 5-l-oxoproline with ChaC2 are −6.3 kcal/mol and −5.2 kcal/mol, respectively. (B) Close-up view of the active site cavity of ChaC2. The ChaC2 E74Q residues recognizing GSH/5-l-oxoproline and catalytic Glu83 are shown as stick models with white and light blue colors, respectively. (C) SPR experiments with ChaC2 E74Q E83Q and GSH. Various concentrations of free GSH were applied to the immobilized ChaC2. Sensorgrams for 1.953, 3.906, 7.813, 15.63, 31.25, and 62.50 μM GSH are shown in different colors. The KD value of GSH to ChaC2 E74Q E83Q was calculated as 2.724 μM

Integrating my above results with previous discoveries of the pivotal binding site residues of GGCAT, I demonstrated mechanism of GSH degradation reaction. In the early step of substrate binding to open binding sites of the enzyme, the swapping-loop region induces domain rearrangements, causes a conformational change and bring Glu74 in close proximity to facilitate proton transfer GSH in the cavity. At the cavity apex, the aromatic side-chains of Tyr6, Tyr89, Tyr109 residues guide, orient GSH, and form a hydrophobic face against the thiol moiety of GSH. When GSH accesses to the catalytic Glu74, it is engaged in a complicated hydrogen bonding network with the active-site residues. In addition, the Gln34, His38, and Arg40 also appear to fix the second and third residue in substrate in an optimum position of GSH in the cavity. The phenyl ring of Tyr144 provides a protective environment for the reactive GSH thiol and is probably involved in correct substrate orientation (Figure 25B).

In starting state of reaction, the amine moieties of Tyr6, Gly7, Ser8, and Leu9 form hydrogen bond with the oxygen atoms of the γ-glutamyl portion of the GSH (Figure 26) and orient γ-glutamyl moiety to the carboxyl group of Glu74. The Glu74 acts as a general acid-base that abstracts a proton from the γ-glutamyl amino group with concomitant nucleophilic attack of the amine onto the side chain amide carbon atom. The resulting oxyanion intermediate collapses to form 5-L-oxoproline. Then the protonated Glu74 donates a hydrogen to amine of the γ-linked peptide, allowing its release with a free amino group. 5-L-oxoproline is released followed by the release of cysteine-glycine (Figure 26)

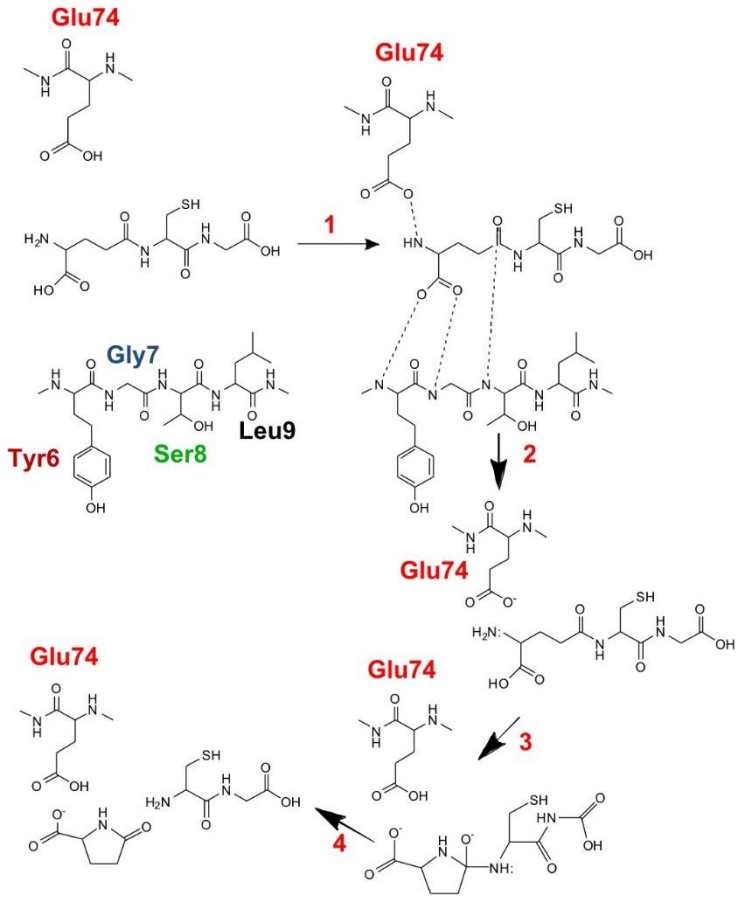

Figure 26. Proposed catalytic mechanism of ChaC2 protein

3. Correlation of ChaC2, GSH degradation, and breast cancer

ChaC family proteins have been considered attractive targets for cancer therapies due to their influence on cancer cell proliferation [25, 28, 53]. Overexpression of ChaC1 increased the proliferation of breast cancer and ovarian cancer cell lines, however, it is not yet fully understood why the overexpression of the ChaC family proteins promotes the proliferation of certain cancer cell lines [25]. Similarly, I also found that the overexpression of ChaC2 in MCF-7 breast cancer cell lines induced cell proliferation. However, the overexpression of ChaC2 mutants at the active site did not induce cell proliferation, unlike ChaC2. In addition, I observed variations of the behavior of ChaC2 and its mutants in MDA-MB-231 breast cancer cell lines (Figure 27). The overexpression of ChaC2 but not ChaC2 E74Q and ChaC2 E83Q promoted MDA-MB-231 breast cancer cell line proliferation, evaluated in an MTT assay (Figure 27).

Taken together, these results indicate that ChaC2 modulates the growth of breast cancer cells via its GSH degradation activity in the GSH metabolism. ChaC2 knockdown has been shown to downregulate Nrf2, a master of the antioxidant response [10]. In breast cancer cells, Nrf2 has been also shown to be overexpressed and promote cell proliferation [60, 61]. Overexpression of ChaC2 mutants at the active site would result in the increase of intracellular GSH level and the inhibition of Nrf2, which would elicit anti-proliferative effects on cancer cells. My findings provide beneficial insights into developing new treatment strategies for breast cancer diseases by inhibiting the glutathione degradation activity of ChaC family enzymes.

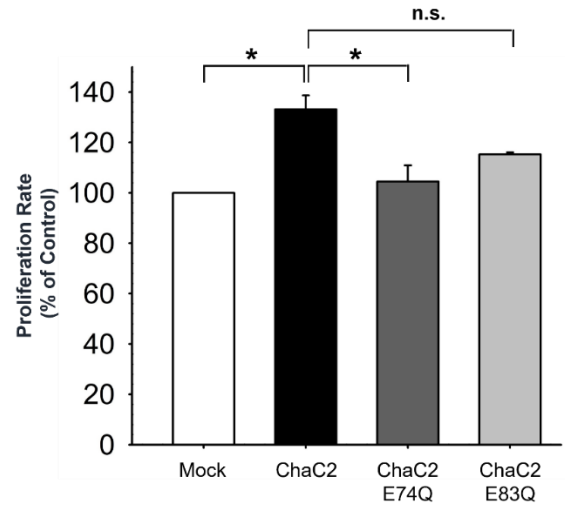

Figure 27. Viability of ChaC2-overexpressed MDA-MB-231 cell line was measured by MTT assay.

The proliferation rate of cells is shown with relative percentages compared to the Mock-transfected cells. Data represent the mean ±SEM (error bars) of three independent experiments. Asterisks indicate statistically significant differences; * $p < 0.05$.

Reference

[1] Liu Y, Hyde AS, Simpson MA, Barycki JJ. Chapter Two - Emerging Regulatory Paradigms in Glutathione Metabolism. In: Townsend DM, Tew KD, editors. Advances in Cancer Research: Academic Press; 2014. p. 69-101.
[2] Messina JP, Lawrence DA. Cell cycle progression of glutathione-depleted human peripheral blood mononuclear cells is inhibited at S phase. The Journal of Immunology. 1989;143:1974-81.
[3] Townsend DM, Tew KD, Tapiero H. The importance of glutathione in human disease. Biomedicine & Pharmacotherapy. 2003;57:145-55.
[4] Bansal A, Simon MC. Glutathione metabolism in cancer progression and treatment resistance. The Journal of Cell Biology. 2018;217:2291-8.
[5] Traverso N, Ricciarelli R, Nitti M, Marengo B, Furfaro AL, Pronzato MA, et al. Role of glutathione in cancer progression and chemoresistance. Oxidative medicine and cellular longevity. 2013;2013:972913-.
[6] Kumar BA, Amandeep K. Glutathione Degradation. Antioxidants & Redox Signaling. 2017;27:1200-16.
[7] Martin MN, Saladores PH, Lambert E, Hudson AO, Leustek T. Localization of Members of the γ-Glutamyl Transpeptidase Family Identifies Sites of Glutathione and Glutathione S-Conjugate Hydrolysis. Plant Physiology. 2007;144:1715-32.
[8] Han B, Luo G, Zheng-Zheng S, Barrios R, et al. Gamma-glutamyl leukotrienase, a novel endothelial membrane protein, is specifically responsible for leukotriene D(4) formation in vivo. The American Journal of Pathology. 2002;161:481.
[9] Wickham S, West MB, Cook PF, Hanigan MH. Gamma-glutamyl compounds: Substrate specificity of gamma-glutamyl transpeptidase enzymes. Analytical Biochemistry. 2011;414:208-14.
[10] Wang C-K, Yang S-C, Hsu S-C, Chang F-P, Lin Y-T, Chen S-F, et al. CHAC2 is essential for self-renewal and glutathione maintenance in human embryonic stem cells. Free Radical Biology and Medicine. 2017;113:439-51.
[11] Oakley AJ, Yamada T, Liu D, Coggan M, Clark AG, Board PG. The Identification and Structural Characterization of C7orf24 as γ-Glutamyl Cyclotransferase: AN ESSENTIAL ENZYME IN THE γ-GLUTAMYL CYCLE. Journal of Biological Chemistry. 2008;283:22031-42.
[12] Oakley AJ, Coggan M, Board PG. Identification and Characterization of γ-Glutamylamine Cyclotransferase, an Enzyme Responsible for γ-Glutamyl-ϵ-lysine Catabolism. The Journal of Biological Chemistry. 2010;285:9642-8.
[13] Kaur A, Gautam R, Srivastava R, Chandel A, Kumar A, Karthikeyan S, et al. ChaC2, an Enzyme for Slow Turnover of Cytosolic Glutathione. Journal of Biological Chemistry. 2017;292:638-51.
[14] Chi Z, Byrne Sean T, Dolinko A, Harraz Maged M, Kim M-S, Umanah G, et al. Botch Is a γ-Glutamyl Cyclotransferase that Deglycinates and Antagonizes Notch. Cell Reports. 2014;7:681-8.
[15] Kumar A, Tikoo S, Maity S, Sengupta S, Sengupta S, Kaur A, et al. Mammalian proapoptotic factor ChaC1 and its homologues function as γ-glutamyl cyclotransferases acting specifically on glutathione. EMBO reports. 2012;13:1095-101.
[16] Qu C, Liljas L, Opalka N, Brugidou C, Yeager M, Beachy RN, et al. 3D Domain Swapping Modulates the Stability of Members of an Icosahedral Virus Group. Structure. 2000;8:1095-103.
[17] Ding F, Dokholyan NV, Buldyrev SV, Stanley HE, Shakhnovich EI. Molecular Dynamics Simulation of the SH3 Domain Aggregation Suggests a Generic Amyloidogenesis Mechanism. Journal of Molecular Biology. 2002;324:851-7.
[18] Vitagliano L, Adinolfi S, Sica F, Merlino A, Zagari A, Mazzarella L. A potential allosteric subsite generated by domain swapping in bovine seminal ribonuclease11Edited by A. R. Fersht. Journal of Molecular Biology. 1999;293:569-77.
[19] O'Neill JW, Kim DE, Johnsen K, Baker D, Zhang KYJ. Single-Site Mutations Induce 3D Domain Swapping in the B1 Domain of Protein L from Peptostreptococcus magnus. Structure. 2001;9:1017-27.
[20] Malevanets A, L. Sirota F, Wodak SJ. Mechanism and Energy Landscape of Domain Swapping in the B1 Domain of Protein G. Journal of Molecular Biology. 2008;382:223-35.
[21] Rousseau F, Schymkowitz JWH, Itzhaki LS. The Unfolding Story of Three-Dimensional Domain Swapping. Structure. 2003;11:243-51.
[22] MacKinnon SS, Wodak SJ. Landscape of Intertwined Associations in Multi-Domain Homo-Oligomeric Proteins. Journal of Molecular Biology. 2015;427:350-70.
[23] Joo NE, Ritchie K, Kamarajan P, Miao D, Kapila YL. Nisin, an apoptogenic bacteriocin and food

preservative, attenuates HNSCC tumorigenesis via CHAC1. Cancer Medicine. 2012;1:295-305.
[24] Mungrue IN, Pagnon J, Kohannim O, Gargalovic PS, Lusis AJ. CHAC1/MGC4504 Is a Novel Proapoptotic Component of the Unfolded Protein Response, Downstream of the ATF4-ATF3-CHOP Cascade. The Journal of Immunology. 2009;182:466-76.
[25] Goebel G, Berger R, Strasak AM, Egle D, Müller-Holzner E, Schmidt S, et al. Elevated mRNA expression of CHAC1 splicing variants is associated with poor outcome for breast and ovarian cancer patients. British Journal of Cancer. 2012;106:189-98.
[26] Crawford RR, Prescott ET, Sylvester CF, Higdon AN, Shan J, Kilberg MS, et al. Human CHAC1 Protein Degrades Glutathione, and mRNA Induction Is Regulated by the Transcription Factors ATF4 and ATF3 and a Bipartite ATF/CRE Regulatory Element. Journal of Biological Chemistry. 2015;290:15878-91.
[27] Nomura Y, Hirata Y, Kiuchi K, Oh-hashi K. Translational and post-translational regulation of mouse cation transport regulator homolog 1. Scientific Reports. 2016;6:28016.
[28] Liu S, Fei W, Shi Q, Li Q, Kuang Y, Wang C, et al. CHAC2, downregulated in gastric and colorectal cancers, acted as a tumor suppressor inducing apoptosis and autophagy through unfolded protein response. Cell Death &Amp; Disease. 2017;8:e3009.
[29] L'Espérance S, Bachvarova M, Tetu B, Mes-Masson A-M, Bachvarov D. Global gene expression analysis of early response to chemotherapy treatment in ovarian cancer spheroids. BMC Genomics. 2008;9:99-.
[30] Bailey HH, Ripple G, Tutsch KD, Arzoomanian RZ, Alberti D, Feierabend C, et al. Phase I Study of Continuous-Infusion l - S,R -Buthionine Sulfoximine With Intravenous Melphalan. JNCI: Journal of the National Cancer Institute. 1997;89:1789-96.
[31] The UniProt Consortium. UniProt: the universal protein knowledgebase. Nucleic Acids Research. 2017;45:D158-D69.
[32] Sievers F, Wilm A, Dineen D, Gibson TJ, Karplus K, Li W, et al. Fast, scalable generation of high-quality protein multiple sequence alignments using Clustal Omega. Molecular Systems Biology. 2011;7:539.
[33] Gouet P, Courcelle E, Stuart D, Métoz F. ESPript: analysis of multiple sequence alignments in PostScript. Bioinformatics (Oxford, England). 1999;15:305-8.
[34] Walden H. Selenium incorporation using recombinant techniques. Acta Crystallographica Section D: Biological Crystallography. 2010;66:352-7.
[35] McGuffin LJ, Bryson K, Jones DT. The PSIPRED protein structure prediction server. Bioinformatics (Oxford, England). 2000;16:404-5.
[36] Rafał A, Aleksey P, Jarosław M. Combining prediction of secondary structure and solvent accessibility in proteins. Proteins: Structure, Function, and Bioinformatics. 2005;59:467-75.
[37] Rhodes DR, Kalyana-Sundaram S, Mahavisno V, Varambally R, Yu J, Briggs BB, et al. Oncomine 3.0: genes, pathways, and networks in a collection of 18,000 cancer gene expression profiles. Neoplasia (New York, NY). 2007;9:166-80.
[38] Otwinowski Z, Minor W. [20] Processing of X-ray diffraction data collected in oscillation mode. Methods in Enzymology: Academic Press; 1997. p. 307-26.
[39] Adams PD, Afonine PV, Bunkoczi G, Chen VB, Davis IW, Echols N, et al. PHENIX: a comprehensive Python-based system for macromolecular structure solution. Acta Crystallographica Section D. 2010;66:213-21.
[40] McCoy AJ, Grosse-Kunstleve RW, Adams PD, Winn MD, Storoni LC, Read RJ. Phaser crystallographic software. Journal of Applied Crystallography. 2007;40:658-74.
[41] Emsley P, Lohkamp B, Scott WG, Cowtan K. Features and development of Coot. Acta Crystallographica Section D: Biological Crystallography. 2010;66:486-501.
[42] Winn MD, Ballard CC, Cowtan KD, Dodson EJ, Emsley P, Evans PR, et al. Overview of the CCP4 suite and current developments. Acta Crystallographica Section D: Biological Crystallography. 2011;67:235-42.
[43] J. WC, J. HJ, W. MN, G. PM, L. VL, N. DL, et al. MolProbity: More and better reference data for improved all-atom structure validation. Protein Science. 2018;27:293-315.
[44] Joosten RP, Salzemann J, Bloch V, Stockinger H, Berglund A-C, Blanchet C, et al. PDB_REDO: automated re-refinement of X-ray structure models in the PDB. Journal of Applied Crystallography. 2009;42:376-84.
[45] Rahman I, Kode A, Biswas SK. Assay for quantitative determination of glutathione and glutathione disulfide levels using enzymatic recycling method. Nature Protocols. 2007;1:3159.
[46] Trott O, Olson AJ. AutoDock Vina: improving the speed and accuracy of docking with a new scoring function, efficient optimization and multithreading. Journal of computational chemistry. 2010;31:455-61.

[47] Wu H-Y, Liu M-S, Lin T-P, Cheng Y-S. Structural and Functional Assays of AtTLP18.3 Identify Its Novel Acid Phosphatase Activity in Thylakoid Lumen. Plant Physiology. 2011;157:1015-25.
[48] Krissinel E, Henrick K. Detection of Protein Assemblies in Crystals. Berlin, Heidelberg: Springer Berlin Heidelberg; 2005. p. 163-74.
[49] Holm L, Rosenström P. Dali server: conservation mapping in 3D. Nucleic Acids Research. 2010;38:W545-W9.
[50] Ran R, Liu Y, Gao H, Kuang Q, Zhang Q, Tang J, et al. PEGylated Hyaluronic Acid-Modified Liposomal Delivery System with Anti-γ-Glutamylcyclotransferase siRNA for Drug-Resistant MCF-7 Breast Cancer Therapy. Journal of Pharmaceutical Sciences. 2015;104:476-84.
[51] Matsumura K, Nakata S, Taniguchi K, Ii H, Ashihara E, Kageyama S, et al. Depletion of γ-glutamylcyclotransferase inhibits breast cancer cell growth via cellular senescence induction mediated by CDK inhibitor upregulation. BMC Cancer. 2016;16:748.
[52] Hiromi I, Taku Y, Susumu N, Keiko T, Koushi H, Shugo T, et al. A Novel Prodrug of a γ-Glutamylcyclotransferase Inhibitor Suppresses Cancer Cell Proliferation in vitro and Inhibits Tumor Growth in a Xenograft Mouse Model of Prostate Cancer. ChemMedChem. 2018;13:155-63.
[53] Jahn B, Arvandi M, Rochau U, Fiegl H, Goebel G, Marth C, et al. Development of a novel prognostic score for breast cancer patients using mRNA expression of CHAC1. Journal of Comparative Effectiveness Research. 2017;6:563-74.
[54] Chen M-S, Wang S-F, Hsu C-Y, Yin P-H, Yeh T-S, Lee H-C, et al. CHAC1 degradation of glutathione enhances cystine-starvation-induced necroptosis and ferroptosis in human triple negative breast cancer cells via the GCN2-eIF2α-ATF4 pathway. Oncotarget. 2017;8:114588-602.
[55] Győrffy B, Lanczky A, Eklund AC, Denkert C, Budczies J, Li Q, et al. An online survival analysis tool to rapidly assess the effect of 22,277 genes on breast cancer prognosis using microarray data of 1,809 patients. Breast Cancer Research and Treatment. 2010;123:725-31.
[56] Golczak M, Sears AE, Kiser PD, Palczewski K. LRAT-specific domain facilitates vitamin A metabolism by domain swapping in HRASLS3. Nature chemical biology. 2015;11:26-32.
[57] Murray AJ, Head JG, Barker JJ, Brady RL. Engineering an intertwined form of CD2 for stability and assembly. Nature Structural Biology. 1998;5:778.
[58] Rousseau F, Schymkowitz JWH, Wilkinson HR, Itzhaki LS. Three-dimensional domain swapping in p13suc1 occurs in the unfolded state and is controlled by conserved proline residues. Proceedings of the National Academy of Sciences. 2001;98:5596-601.
[59] Taylor CAt, Juang Y-C, Earnest S, Sengupta S, Goldsmith EJ, Cobb MH. Domain-Swapping Switch Point in Ste20 Protein Kinase SPAK. Biochemistry. 2015;54:5063-71.
[60] Zhang C, Wang H-J, Bao Q-C, Wang L, Guo T-K, Chen W-L, et al. NRF2 promotes breast cancer cell proliferation and metastasis by increasing RhoA/ROCK pathway signal transduction. Oncotarget. 2016;7:73593-606.
[61] Zhang H-S, Du G-Y, Zhang Z-G, Zhou Z, Sun H-L, Yu X-Y, et al. NRF2 facilitates breast cancer cell growth via HIF1α-mediated metabolic reprogramming. The International Journal of Biochemistry & Cell Biology. 2018;95:85-92.

Abstract in Korean

Glutathione(GSH)의 분해는 GSH의 항상성을 유지할 뿐만 아니라, 암세포에서 세포 생존에 중요한 역할을 한다고 알려져 있다. 특히 GSH 분해를 담당하는 효소들 중 ChaC1과 ChaC2는 공통적으로 GSH를 분해하여 5-L-oxoproline 과 Cys-Gly 펩타이드를 만드는 역할을 하는데, 서로의 아미노산 서열은 60% 정도 유사하다고 알려져 있다. 본 연구에서는 ChaC2의 각각 다른 두 가지 형태의 결정 구조를 밝혔고, 이 구조들을 기존에 알려져 있던 다른 γ-glutamylcyclotransferase 계열의 효소들과 비교하였다. ChaC2 결정 구조에서 발견되는 domain-교환 loop은 GSH와의 결합 특이성을 부여하는 부분으로, GSH 분해 속도를 조절하는 데 중요한 역할을 하는 것으로 보인다. 여러 생화학적인 실험 결과와 단백질 구조 분석을 통하여 Glu74와 Glu83이 이합체의 형성과 단백질 활성의 조절에 중요한 역할을 한다는 것을 알 수 있었고, GSH와 ChaC2 사이의 docking 연구와 결합 실험을 통해 GSH와 ChaC2의 사이의 결합 방식과 ChaC2의 반응 메커니즘을 제시하였다. 뿐만 아니라, ChaC2의 과발현이 E74Q와 E83Q 변이 단백질들에 비해 유방암 세포의 생존을 증가시키는 실험 결과를 토대로 ChaC2에 의한 GSH의 분해가 유방암의 발달에 특정 역할을 할 것이라 제시할 수 있었다.

결과적으로, ChaC2의 구조와 기능에 대한 본 연구는 ChaC 계열 단백질들을 조절할 수 있는 분자의 개발에 기여하고, 더 나아가 GSH 분해와 관련된 질병과 암을 효율적으로 조절할 수 있는 치료의 기반을 제공한다.

Acknowledgements

Firstly, I would like to express my sincere appreciation to my supervisor Prof. Byung Woo Han for his continuous supporting, his patience, encouragement, motivation, and immense knowledge during my PhD years. Thanks for his nice adoption me to his Korean lab, where I learnt everything, including Korean culture, Korean language, lab life, scientific life, and so on. I think he is the most positive Professor I have ever met. I was impressed the way he treats and cares students so that he makes Korea like my second family. I am also really appreciated for his understanding and empathizing my hard time in Korea and research!!

Beside of my supervisor, I would like to thank my thesis committee: Prof. Jung Weon Lee, Prof. Young-Joon Surh, and Prof. Marc Diederich for the kind comments which incented me to widen and solidify my research from various perspectives.

I really want to thank my senior Dr. Kyung Rok Kim who taught me very first techniques in molecular biological research and gave me considerable care for my life and study in Korea. He has endured and sacrificed his time to teach and fix the mistake in my research experiments. He always provided me great ideas to overcome research trouble-shooting. Thank for giving me a lot of advices to improve my skill when things got rough and encouraging me a lot with his optimistic perspectives. He shared and helped me to understand the Korean culture, lab culture, and enjoyed the Korean life. Therefore, I always feel close to my Lab members!

My great thanks also to Dr. Joon Sung Park who constantly supported and encouraged me during the PhD course. He also shared a lot of experience, tips in the experiments with his very detail and understandable explanation. I want to give my sincere thanks to him for the sleepless nights we were working together before deadlines. He guided me for the project research and revised my manuscripts. Without his help I could not have imagined having a better research and knowledge.

I would like to thank Dr. Jun Young Jang who always asked my research process, prayed for good thing to our lab, and for me in Korea.

Thank to my senior, Dr. Hyunggu Han, who is the first one picked up me at the Korea Airport and escorted me safely in the first day in Korea. He had been studied abroad like me so he was one understanding my difficulty in Korea. He has been helping me both in Korean life and research life. Especially, he is my English teacher, as well. Thanks for his kind help for English editing for any document, material, manuscript, and conference in English.

I want to show my great thank to Dr. Hyoun Sook Kim. Thanks for kind helping me in experiments, especially protein structure experiments since I was very navy in this field. She is the female scientist who I admired the most and motivated me during PhD course. I am pretty sure she will be the most inspired lady I have been met in my life!

I also thank my junior, Jang Dong Man who shared with me many funny moments to release depression and gave me free help in Korean life. He is very kind, friendly, warm, care, positive, and humorous to every lab-members, which encouraged me a lot to become a positive one living in Korea.

In addition, I also want to thank my Vietnamese friends in Korea, including my close friends in “Ba chi em va co em gai e” group and SNU badminton club who were always beside and shared with me great time outside the Lab time.

Lastly, my sense of gratitude to my family, especially my mother, my sister, and my younger brother for supporting me spiritually throughout my life. My mom who understands and supports for my dream to learn biotechnology and bring it to my country.